Title page

GPR30 in spinal cholecystokinin-positive neurons modulates neuropathic pain via mediating descending facilitation

Qing Chen[1#], Hui Wu[1#], Shulan Xie[1#], Fangfang Zhu[1], Fang Xu[2], Qi Xu[1], Lihong Sun[1], Yue Yang[3], Linghua Xie[1], Jiaqian Xie[4], Hua Li[1], Ange Dai[1], Wenxin Zhang[1], Luyang Wang[1], Cuicui Jiao[1], Honghai Zhang[4], Zhen-Zhong Xu[5,6*], Xinzhong Chen[1*].

[1]Department of Anesthesia, Women's Hospital, Zhejiang University School of Medicine, Hangzhou, 310006, China.

[2]Department of Anesthesiology, The Second Affiliated Hospital, Chongqing Medical University, Chongqing, 400010, China.

[3]Department of Anesthesiology, Affiliated Hangzhou First People's Hospital, Westlake University School of Medicine, Hangzhou, 310006, China.

[4]Department of Anesthesiology, Sir Run Run Shaw Hospital, School of Medicine, Zhejiang University, Hangzhou, 317500, China.

[5]Department of Anesthesiology, First Affiliated Hospital and School of Brain Science and Brain Medicine, Zhejiang University School of Medicine, Hangzhou, 310058, China.

[6]Liangzhu Laboratory, MOE Frontier Science Center for Brain Science and Brain-machine Integration, State Key Laboratory of Brain-machine Intelligence, NHC and CAMS Key Laboratory of Medical Neurobiology, Zhejiang University, Hangzhou, 311121, China

[#]These authors contributed equally.

***Correspondence:** Chen Xinzhong, M.D., Department of Anesthesia, Women's Hospital, Zhejiang University School of Medicine, Hangzhou, 310006, China.

E-mail: chenxinz@zju.edu.cn. Tel: +86-571-87061501.

Fax: +86-571-87061878

****Correspondence:** Xu Zhen-Zhong, PhD, Department of Neurobiology and Anesthesiology of First Affiliated Hospital, Zhejiang University School of Medicine, Hangzhou, 310058, China

E-mail: xuzz@zju.edu.cn

Abstract

Neuropathic pain, a major health problem affecting 7 - 10% of the global population, lacks effective treatment due to its elusive mechanisms. Cholecystokinin-positive (CCK^+) neurons in the spinal dorsal horn (SDH) are critical for neuropathic pain, yet the underlying molecular mechanisms remain unclear. Here we showed that the membrane estrogen receptor G-protein coupled estrogen receptor (GPER/GPR30) in spinal was significantly upregulated in chronic constriction injury (CCI) mice and that inhibition of GPR30 in CCK^+ neurons reversed CCI-induced neuropathic pain. Besides, GPR30 in spinal CCK^+ neurons was essential for the enhancement of AMPA-mediated excitatory synaptic transmission in CCI mice. Furthermore, GPR30 was expressed in the spinal CCK^+ neurons receiving direct projection from the primary sensory cortex (S1-SDH). Chemogenetic inhibition of S1-SDH post-synaptic neurons alleviated CCI-induced neuropathic pain. Conversely, chemogenetic activation of these neurons mimicked neuropathic pain symptoms, which were attenuated by spinal inhibition of GPR30. Finally, we confirmed that GPR30 in S1-SDH post-synaptic neurons is required for CCI-induced neuropathic pain. Taken together, our findings suggest that GPR30 in spinal CCK^+ neurons is pivotal for neuropathic pain and mediates descending facilitation by corticospinal direct projections, thereby representing a promising therapeutic target for neuropathic pain.

Key words: corticospinal direct projections, descending facilitation, GPR30, neuropathic pain, spinal CCK positive neurons

Introduction

Neuropathic pain is a common chronic pain condition caused by a lesion or dysfunction of the somatosensory nervous system and affects nearly 7-10% of the population worldwide[1-4]. Neuropathic pain is characterized by mechanical allodynia, under which innocuous stimuli can produce pain, and thermal hyperalgesia where normally painful stimuli produce more intense pain[1,5,6]. However, the complicated and elusive mechanisms of neuropathic pain still make it difficult to treat. Thus, it is urgent for us to identify exact mechanisms of neuropathic pain and discover new therapeutic targets.

Since the spinal cord (SC) is a major site for integration of peripheral sensory information and receiving descending modulation from higher center, neuropathic mechanical allodynia occurs via circuit-based transformation in this remarkable region[4,5,7,8]. The superficial laminae of SC are responsible for the noxious perception while the deeper laminae are important for innocuous perception. However, under neuropathic conditions, the low-threshold mechanosensory stimulation would also activate nociceptive neurons localized in the superficial laminae under the mechanism of disinhibition and sensitization, thus resulting in mechanical allodynia. Excitatory interneurons cover a majority proportion of neurons (nearly 75%) in the spinal dorsal horn (SDH) and are thought to take a vital role in neuropathic pain[9-11]. Cholecystokinin-positive (CCK^+) neurons are recently reported to be an important subtype of excitatory interneurons widely distributed in the deep laminae of the SDH and to play a crucial role in mediating mechanical allodynia and thermal hyperalgesia[10,12]. Of great interest is that CCK^+ neurons also receive direct top-down projections from S1 cortex which have been reported to modulate neuropathic pain

sensitivity[13]. However, little is known about the molecular mechanisms underlying the contribution of CCK^+ neurons to neuropathic pain modulation.

Estrogen has been repeatedly verified to take a vital role in nociceptive modulation at peripheral and central level[14-21]. Besides of its nuclear receptors-estrogen receptor α (ERα) and estrogen receptor β (ERβ), estrogen can produce various physiological and pathological effects by non-genetic pathways via membrane receptor-G protein-coupled estrogen receptor (GPR30)[22,23]. Interestingly, GPR30 has been reported by several studies to be involved in pain modulation[16 24,25,26]. However, it is still unclear whether GPR30 in the SDH plays a critical role in the modulating neuropathic pain.

In this study, we identified that GPR30 in spinal CCK^+ neurons modulates neuropathic pain and mediates the descending facilitation by sensory cortex-spinal cord direct projection. We discovered that GPR30 activation in spinal CCK^+ neurons was both required and sufficient for the development of neuropathic pain. Interestingly, we found that GPR30 in spinal CCK^+ neurons was required for the enhancement of spontaneous excitatory post-synaptic currents (sEPSC) in CCI mice, in an AMPA-dependent manner. Importantly, we further revealed that GPR30 was expressed in the spinal CCK^+ neurons receiving direct projections from S1 sensory cortex and GPR30 in S1-SDH post-synaptic neurons was critical for CCI-induced neuropathic pain. Thus, our results suggest that GPR30 in spinal CCK^+ neurons is a promising therapeutic target for treating neuropathic pain.

Results

Spinal inhibition of GPR30 reverses CCI-induced neuropathic pain and neuronal activation

To assess the potential role of spinal GPR30 in the development of neuropathic pain, we investigated whether spinal inhibition of GPR30 could relieve neuropathic pain induced by CCI (chronic constriction injury) nerve injury model (Fig 1A). Quantitative PCR (qPCR) revealed that mRNA expression of *Gper1* (GPR30) in lumbar SDH was upregulated in CCI mice (Fig 1B). The intrathecal application of G-15, an antagonist of GPR30, significantly reversed the mechanical allodynia and thermal hyperalgesia induced by CCI in both genders of mice (Fig 1C-E). While intrathecal application of G-15 did not change the basal pain threshold in naïve mice (Fig S1A and B). Of note, the analgesic effects of G-15 lasted for up to 6 hours after intrathecal application in CCI mice (Fig S1C). Immunochemistry data showed that light touch induced robust increase of c-Fos (a neuronal activation marker) expression, mainly in GPR30^{+} cells, in the SDH of male and female CCI mice (Fig 1F-J). Furthermore, intrathecal injection of G-15 largely reversed c-Fos activation in CCI mice, suggesting that spinal inhibition of GPR30 reversed CCI-induced neuropathic pain and neuronal activation in both genders (Fig 1F-J).

Next, we tested whether spinal activation of GPR30 could mimic neuropathic pain symptoms in naïve mice. Indeed, intrathecal application of selective GPR30 agonist G-1 dramatically induced mechanical allodynia and thermal hyperalgesia in both genders of mice (Fig S1D-F), which could persist for over 48 hours (Fig S1G). Moreover, immunochemistry results showed that the number of c-Fos^{+} neurons (>80% in GPR30^{+} cells) in the SDH significantly increased by spinal activation of GPR30 (Fig S1H-J).

Therefore, these data demonstrate that activation of spinal GPR30 is essential for CCI-induced neuropathic pain in both genders of mice.

GPR30 in spinal CCK$^+$ neurons is required for CCI-induced neuropathic pain

Then we tried to find out which groups of spinal cells are targeted by GPR30 in pain modulation. As shown in the results, GPR30 was almost exclusively expressed in the neuronal cells of SDH instead of astrocytes or microglial cells (Fig. S2). It should be noted that, as an estrogen receptor, GPR30 is indiscriminately expressed in both genders of mice (Fig S2A). In addition, further results revealed that GPR30 was mainly expressed by excitatory interneurons of SDH as labeled by AAV2/9-Camk2-mCherry in WT mice (Fig 2A and B).

As mentioned before, it is well-established that spinal CCK$^+$ neurons are involved in light touch perception and pain modulation during neuropathic pain[10,21]. By the way, CCK$^+$ neurons cover a large part of excitatory interneurons in the SDH[27,28]. Thus, we intended to explored whether CCK$^+$ neurons modulate neuropathic pain via GPR30 and the involved mechanisms. CCK expression was characterized in the spinal cord by crossing of *CCK-Cre* mice with *Ai14* mice (Fig 2C). ISH and immunochemistry studies confirmed that our transgenic mice recapitulated the majority of *CCK* expression in the deep laminae of the SDH as marked by isolectin B4 (IB4) (Fig 2D-E). Immunochemistry results showed that GPR30 was expressed by almost all CCK$^+$ neurons in the SDH (Fig 2F).

Confirmed the structural connections between GPR30 and CCK$^+$ neurons, we next explored whether GPR30 in CCK$^+$ neurons had a vital role in neuropathic pain. We injected AAV2/9-DIO-shGper1-EGFP into the lumbar SDH of *CCK-Cre* mice to knock down the expression of *Gper1* in CCK$^+$ neurons, and 3 weeks later mice were subjected to CCI and subsequent behavioral tests (Fig 3A). The immunochemistry confirmed the location of virus in the deep laminae of SDH which is consistent with the distribution of CCK$^+$ neurons (Fig

3B). Knock down of *Gper1* in lumbar spinal CCK^+ neurons significantly suppressed the increased expression of *Gper1* mRNA by CCI in mice (Fig 3C, Fig S3A).

We next tested whether GPR30 expressed on CCK^+ neurons was essential for CCI-induced pain-like behaviors. As expected, the knockdown of *Gper1* in CCK^+ neurons significantly attenuated mechanical allodynia and heat hyperalgesia induced by CCI in both genders of mice (Fig 3D-F). But it should be noted that, knockdown of *Gper1* in CCK^+ neurons alone did not change the basic mechanical nociceptive threshold (Fig 3D-F). To further determined whether GPR30 in CCK^+ neurons is involved in the affective components of neuropathic pain, we used real-time PEA test with innocuous mechanical stimulation as shown before[2](Fig 3G). As shown in the results, CCI mice treated by scramble spent less time on the stimulated side and exhibited an aversive response even during the post-stimulation period, while *Gper1* knockdown mice with CCI did not show any aversive behaviors (Fig 3H-L).

GPR30 in spinal CCK^+ neurons is essential for the enhancement of excitatory synaptic transmission in the SDH of CCI mice

To determine how GPR30 expressed on CCK^+ neurons mediated the nociception of neuropathic pain, we recorded from fluorescently labeled cells with whole-cell patch clamp recording in spinal slices from CCI or sham *CCK-Cre* mice treated by shRNA (Fig 4A and B). Since it has been reported that a large part of spinal CCK^+ neurons exhibit excitatory synapses with upstream neurons, we mainly recorded postsynaptic currents from GFP labeled CCK^+ neurons in laminae III-V two weeks after the CCI surgery. Consistent with our speculation, the amplitude but not frequency of excitatory postsynaptic currents (EPSCs) in CCK^+ neurons

were significantly increased by CCI compared to sham (Fig 4C-E). Importantly, this increase of amplitude was absent in *Gper1* knockdown mice (Fig 4C, E). By the way, it should be noted that the inhibitory postsynaptic currents (IPSCs) also took an important role in regulation of neuronal excitability. However, the knockdown of *Gper1* did not influence the IPSCs of spinal CCK^+ neurons in CCI mice (Fig S3B-D).

Known that EPSCs are mediated by glutamatergic receptors like AMPA receptors and several studies have been reported the relationship between GPR30 and AMPA receptor[25,29], we next explored whether the EPSCs mediated by GPR30 depends on AMPA receptor. We performed whole-cell patch clamp recording in spinal slices from *CCK-Cre* mice treated by intraspinal injection of AAV2/9-DIO-EGFP, and a stimulating electrode was applied in the deep laminae of SDH to induce AMPA-dependent currents (Fig 4F and G). All cells were reacting to the stimuli of electrode and present evoked EPSCs (Fig 4H and I). The application of G-1 could further increase the amplitude of AMPA-currents (Fig 4H and I). Together, GPR30 regulate the EPSCs of CCK^+ neurons in an AMPA-dependent manner.

GPR30 is expressed in the spinal CCK^+ neurons receiving direct projection from S1 cortex

To anatomically verify that lumbar spinal receives direct descending projections from the S1 cortex, we used both retrograde (Fig 5A) and anterograde tracing methods (Fig 5D) to identify the cortical neurons and their axonal innervation in the spinal dorsal horn. Our neuronal labeling results showed that retrograde cholera toxin subunit B-555 (CTB-555) injected into the deep laminae of lumbar spinal cord mainly labeled neurons in the contralateral S1 cortex (Fig 5B and C). It should be noted that the projecting neurons residing

in S1 cortex are mainly excitatory pyramidal neurons located in layer V[30]. Similarly, the axons from S1 labeled by AAV2/9-hSyn-EGFP mostly terminated in laminae III-V of the contralateral SDH (Fig 5E and F).

Previous studies suggested a functional connection between S1-SDH projections and spinal CCK^+ neurons[13], here we intend to further verify the structural connections. We injected antegrade trans-monosynaptic AAV2/1-hSyn-Cre into right S1 and then injected AAV2/9-DIO-mCherry into the contralateral lumbar SDH to visualize the $mCherry^+$ S1-SDH post-synaptic neurons in deep laminae of lumbar SDH (Fig 5G and H). In consistency with previous results, we observed that these SDH downstream neurons significantly co-localized with the CCK^+ neurons, with 28.1% mCherry positive neurons expressing *CCK* (Fig 5I and J). Thus, our results confirmed that spinal CCK^+ neurons receive direct projections from S1 cortex.

Then we explored the possible connections among GPR30, S1-SDH projections and CCK^+ neurons. We injected antegrade trans-monosynaptic AAV2/1-EF1α-FLP into right S1 cortex and then injected FLP- and Cre- dependent AAV2/9-hSyn-Con/Fon-GFP into the contralateral lumbar SDH of *CCK-Cre* mice to visualize the GFP-positive S1-SDH post-synaptic CCK^+ neurons (Fig. 5K and L). Importantly, co-staining results showed that nearly all CCK^+ S1-SDH post-synaptic neurons expressed GPR30 (Fig 5M and N). Together, these data demonstrated that the majority of CCK^+ neurons receiving S1 projections expressed GPR30.

GPR30 in S1-SDH post-synaptic neurons is critical for CCI-induced neuropathic pain

Given that GPR30 has been verified to be expressed on CCK^+ neurons receiving S1-SDH

direct projections (Fig 5M), we then used chemogenetic and pharmacological methods to determine whether neurons innervated by S1-SDH direct projections mediate nociception via GPR30. We injected anterograde AAV2/1-hSyn-Cre into right S1 of WT mice, then injected AAV2/9-hSyn-DIO-hM3Dq (Gq)-mCherry into the lumbar SDH one week later (Fig 6A). Pharmacological activation of these post-synaptic neurons by CNO application in Gq-treated mice could induce obviously more spontaneous pain-like behaviors including scratching, biting and licking of hind paws and the tail (Fig 6B). Besides, chemogenetic activation of S1-SDH post-synaptic neurons dramatically induced mechanical allodynia and thermal hyperalgesia in both genders compared to negative control mice (Fig 6C-E). What's more, the decreased nociceptive mechanical and thermal threshold could be relieved by the intrathecal injection of G-15 (Fig 6C-E). The immunochemistry results of c-Fos confirmed the chemogenetic activation of S1-SDH post-synaptic neurons which could be suppressed by the intrathecal application of G-15 (Fig 6F-H).

To examine whether S1-SDH post-synaptic neurons had a role in neuropathic pain modulation, we also used chemogenetic inhibitory methods to suppress these neurons in CCI mice (Fig S4A). The suppression of S1-SDH post-synaptic neurons could dramatically relieve the mechanical allodynia and thermal hyperalgesia induced by CCI (Fig S4B-D). To further confirm whether GPR30 is necessary for S1-SDH post-synaptic neurons to modulate neuropathic pain, we specifically knock down the expression of *Gper1* on S1-SDH post-synaptic neurons and subjected mice to CCI after adequately viral expression (Fig 7A). Interestingly, knockdown of *Gper1* in S1-SDH postsynaptic neurons was sufficiently to relieve the mechanical allodynia and thermal hyperalgesia in both genders (Fig 7B-D).

Immunochemistry showed the viral location in deep laminae of SDH (Fig 7E) and qPCR confirmed the suppression of Gper1 mRNA expression which was increased by CCI (Fig 7F). All these data confirmed that GPR30 played a vital role in the descending facilitation of S1-SDH direct projections in neuropathic pain.

Discussion

CCK^+ neurons, located in the deep laminae of SDH, has long been confirmed to take a pivotal role in neuropathic pain and descending facilitation by sensory cortex-spinal cord projections, yet little is known about its molecular mechanisms underlying nociception. GPR30, as a membrane estrogen receptor, could exerts modulatory effects within seconds to minutes on various physiological and pathological conditions including neuropathic pain[22]. In this study, we discovered that spinal GPR30 expression was significantly upregulated after CCI and is vital for the development of neuropathic pain. Then we used transgenic mice, behavioral testing, pharmacological methods, chemogenetic methods and electrophysiological methods to further demonstrate that GPR30 in spinal CCK^+ neurons takes an indispensable role in neuropathic pain via regulating AMPA-dependent EPSCs. Furthermore, we also confirmed that GPR30 is vital for the descending facilitation by corticospinal direct projections for the development of neuropathic pain. Thus, our data indicates that GPR30 in spinal CCK^+ neurons might represent a promising therapeutic target for neuropathic pain.

Estrogen has long been found to take a predominant role in nociception, especially its drastic fluctuation could dramatically change the nociceptive thresholds[31]. However, the regulatory effects of estrogen in nociception were discriminative. Our previous studies found that moderate supplementation of estrogen could alleviate the hyperalgesia in ovariectomized (OVX) mice, while excessive supplementation of estrogen could further aggravate the

hyperalgesia[31]. The discrepancy might result from that different concentrations of estrogen activate different kinds of estrogen receptors, including nuclear estrogen receptors (ERα and ERβ) and membrane estrogen receptors (GPR30)[22]. With the consideration of our results that inhibition of spinal GPR30 fail to change the basic nociception of naïve mice, GPR30 might be less activated by estrogen in normal condition. Estrogen also has long been reported to have modulatory effects in neuropathic pain. Intra-dorsal root ganglion (DRG) administration of estrogen could promote mechanical and thermal pain in CCI rats via an ERα-dependent manner[32]. Meanwhile, the supplementation of estrogen in ACC could dramatically alleviate neuropathic hyperalgesia in CCI mice in a GPR30-dependent manner[33]. These results further confirm the discriminative roles of different estrogen receptors.

GPR30 is widely expressed in the nervous system and exerts vital effects in nociceptive modulation[16,23,24,33-37]. For example, the activation of GPR30 in DRG could aggravate the hyperalgesia in OVX mice, while inhibition of GPR30 relieved hyperalgesia[38]. Besides, the GPR30 expressed on GABAergic cells in rostral ventromedial medulla (RVM) mediates the descending facilitation of nociception[24]. However, though GPR30 is also widely expressed in SDH[26], still little is known about the functions as well as underlying mechanisms of spinal GPR30 in nociceptive modulation. Consistent with previous studies[39], here we found that intrathecal injection of G-1 could dramatically induce mechanical allodynia and thermal hyperalgesia in mice. To further explore whether spinal GPR30 is involved in pathological nociception, we subjected mice to CCI surgery to mimic neuropathic pain[2,40]. In accordance with our expectations, the inhibition of spinal GPR30 significantly reversed the mechanical allodynia and thermal hyperalgesia induced by CCI. It should be noted that female is more

susceptible to pain than man in clinical practice[41], which could attribute to the mediation of estrogen and its receptors including GPR30. Moreover, GPR30 has been reported to be involved in nociceptive sexual dimorphism. For example, the regulatory role of GPR30 in DRG in maintenance of hyperalgesia induced by repeated exposure of opioid only exists in female rats[42,43]. However, the function spinal GPR30 in nociceptive modulation showed no sexual difference according to our results. Besides, we also found that nearly all GPR30 is indiscriminately expressed on the neurons of both genders of mice and that the proportion of activated $GPR30^{+}$ neurons is similar in CCI mice of both genders, which might account for the sex-independent function of spinal GPR30 in nociceptive modulation. Consistent with our results, several studies also have confirmed that the spinal *Gper1* expression showed no significant difference between male and female mice[44]. What's more, the fluctuation of estrogen failed to change the basic expression of spinal GPR30[31]. These results further indicate the sex-independent function of spinal GPR30 in nociception.

The SDH is a major locus for the integration of peripheral sensory input and supraspinal modulation. Most peripheral nociceptive afferents project to the superficial laminae of the SDH which respond to the noxious stimulations, while low-threshold mechanoreceptors form synaptic contacts in the deep laminae which respond to innocuous stimulations[8]. However, under the condition of mechanical allodynia, innocuous stimulation might also activate more superficial nociceptive circuits and lead to painful perception, which might come from the circuit-based transformation in the SDH[6,45]. It should be noted that the spinal dorsal horn is composed of a large number of excitatory (75%) and inhibitory (25%) interneurons, as well as a small part of projection neurons which relay integrated information to various supraspinal

regions[9]. Excitatory interneurons have been confirmed to take a vital role in conveying mechanical allodynia according to the nature of injury[10]. Calretinin neurons convey mechanical allodynia induced by inflammatory injuries, while protein kinase C gamma neurons convey mechanical allodynia induced by neuropathic injuries[10,46]. As a distinct type of excitatory interneurons mainly located in the deeper laminae of SDH, CCK^+ neurons are important for neuropathic injuries[10-12]. The inhibition of spinal CCK^+ neurons could alleviate neuropathic mechanical allodynia to a great extent[10]. By the way, spinal CCK^+ neurons also account for the thermal hyperalgesia[12]. However, little is known how CCK^+ neurons mediate the nociception. Combined with our results that GPR30 is mainly expressed in spinal excitatory interneurons and involved in neuropathic pain modulation, we speculate that CCK^+ neurons might be convey neuropathic hyperalgesia depending on GPR30. As expected, most CCK^+ neurons express GPR30 and knock-down of the *Gper1* in CCK^+ neurons dramatically relieve the pain induced by CCI, thus indicating the vital role of GPR30 in CCK^+ neurons mediating neuropathic pain.

Abnormal activation of neurons in SDH is one of the causes of hyperalgesia and the change of post synaptic currents is the vital factor influencing neuronal excitability[29,47]. Our electrophysiological results showed the elevation of EPSCs amplitudes in spinal CCk^+ neurons after CCI, indicating the increased excitability of CCK^+ neurons in CCI mice. Furthermore, the knock-down of *Gper1* in CCK^+ neurons could inhibit the increase of EPSCs amplitude. induced by CCI. Together, these data illustrate that GPR30 take a vital role in activation of CCK^+ neurons after nerve injury via promoting the enhancement of EPSCs. It should be noted that EPSCs are specifically produced by glutamatergic receptors expressed on

post-synaptic membrane[48]. Indeed, it has been reported that the GPR30 exerts its effects by regulating the functions of AMPA or NMDA receptors[25,29]. In our study, we confirmed that the selective activation of GPR30 by G-1 remarkedly enhanced the AMPA-current in spinal CCK^+ neurons, which might account for the increased excitability of CCK^+ neurons in neuropathic pain. It should be noted that the IPSCs could also influence the excitability of neurons, however, the knockdown of *Gper1* failed to change the IPSCs amplitude in CCI mice, suggesting that GPR30 did not take part in the inhibitory synaptic regulation.

Increasing evidence has mapped neural circuits from peripheral to central nervous system to illustrate the neural mechanisms of nociception[5,7-9,46,49]. In brief, pain is derived from the activation of peripheral nociceptors whose cell bodies lie in DRG, and then nociceptive signals are transduced to the SDH for preliminary regulation and finally projected to cerebral cortex via a series of brain region mediating nociception. In addition to the ascending pathways mentioned above, pain is also modulated by the descending modulatory pathways constituted of projections from ventrolateral periaqueductal gray (PAG) to the RVM and then to the spinal cord which takes several steps[50-55]. However, A recent study has come up with the existence of long direct projections form S1 cortex to deep laminae of SDH and the vital role of S1-SDH projections in neuropathic pain[13]. Inhibition of S1-SDH projections or transection of corticospinal tract could dramatically attenuate the neuropathic pain induced by spared nerve injury (SNI), while activation of these projections significantly decreases the nociceptive thresholds of naive mice. Consistent with previous studies, we confirmed the existence of S1-SDH direct projections and found that the S1-SDH post-synaptic neurons took an important role in neuropathic pain modulation. Of great interest is that S1-SDH long

direct projections terminate in the deep laminae of the SDH and have functional connections with CCK^+ neurons[13]. Activation of spinal terminals of S1 cortex could increase the activity of CCK^+ neurons. We also structurally verify that CCK^+ neurons receive direct projections from S1 cortex. Furthermore, we also found that the majority of CCK^+ neurons receiving S1-SDH projections express GPR30, thus indicating an important role of GPR30 in descending modulation of S1-SDH. As expected, the knockdown of *Gper1* in S1-SDH post-synaptic neurons dramatically alleviated the hyperalgesia induced by CCI. All these results further confirmed an important role of GPR30 in descending facilitation of neuropathic pain.

Conclusion

our study demonstrates that GPR30 in CCK^+ neurons is essential for the development of neuropathic pain. Furthermore, we revealed that GPR30 is critical for the enhancement of AMPA-dependent EPSCs which promotes the activation of CCK^+ neurons and subsequent abnormal nociception under neuropathic conditions. Additionally, we also discovered that GPR30 is pivotal for the descending facilitation by corticospinal projections in neuropathic pain. Our results suggested that inhibition of GPR30 in spinal CCK^+ neurons could significantly relieve neuropathic pain via blockage the enhancement of AMPA-mediated EPSCs and S1-SDH descending facilitation under neuropathic conditions. GPR30 in spinal CCK^+ neurons might be a promising therapeutic target for neuropathic pain in clinic.

Materials and methods

Animals

Mice of both genders ranging in age from 8 weeks to 12 weeks were used for this study,

including C57BL/6JRJ wild-type (purchased from SLAC Laboratory Animal CO. LTD, Shanghai, China), *CCK-Cre* mice and *Ai14* mice (originally purchased from Jackson Laboratory). In accordance with the Jackson Laboratory's protocol, transgenic mice were genotyped. All animals were kept in a humidity-controlled room with free access to food and water, the facility was maintained at 22 ℃ and ran on 12 hours of light/dark cycles. A random assignment of animals to different experiment groups was conducted. The animals were treated in accordance with protocols approved by the Animal Ethic and Welfare Committee of Zhejiang University School of Medicine, and all experimental procedures were carried out in accordance with the National Institute of Health Guide for Care and Use of Laboratory Animals (NIH Publications NO.86-23).

Drug administration

For pharmacological manipulation of the activity of spinal GPR30, G-1 or G-15 (100 μg/kg, 10 μL per mice; APExBIO, USA) was dissolved in 1% DMSO with Saline and administered intrathecally as previously described[39]. To be specific, mice were lightly anesthetized with 1.5% inhaled isoflurane, and held with a pen under the pelvis while a 25-gauge needle attached to a 10-μL syringe (Hamilton, Nevada, USA) was inserted in the subarachnoid space between vertebrae L5 and L6 until a tail flick was observed. The syringe was held for 30 seconds after the injection of 10 μL solution per mice. For chemogenetic manipulation of S1-SDH post-synaptic neurons, Clozapine N-oxide (CNO; 2.5 mg/kg, 150 μL per mice; MCE, China) was dissolved in saline with gentle vortex for mixing and then administered intraperitoneally[56]. Behaviors were assessed 30 minutes after injection.

Virus and CTB microinjection

For intracranial injection, mice were anesthetized with 1% pentobarbital sodium solution (70 mg/kg per mice) and then secured in a stereotaxic frame (RWD Life Science, Shenzhen, China). A middle scalp incision exposed the skull, and then a hole was drilled on the skull above the right S1 cortex to allow passage of a glass microelectrode filled with the virus. Viral injections were performed with the following coordinates of S1: 0.95~1.15 mm from bregma, 1.4~1.6 mm from midline, and 0.9~1.1 mm ventral to skull. A volume of 300 nL virus was injected at 50 nL/min with calibrated glass microelectrodes by a microsyringe pump (#78-8710 KD Scientific, USA). After infusion, the micropipette was slowly removed after five minutes. For spinal cord injection, mice were anesthetized with 1% pentobarbital sodium solution. The spinal cord could be visible between T12 and T13 vertebral spines following a middle incision along the lumbar vertebrae. With a stereotaxic frame, a glass microelectrode was inserted between L3-L4 spinal cord to a depth of -400 um below the dura, avoiding the posterior spinal arteries. With a stereotaxic injector, 500 nL of viral solution or CTB-555 (1% in PBS; BrainVTA, Wuhan, China) was slowly infused over a period of 5 minutes. The micropipette was left in place for 5 minutes after infusion before being slowly removed.

For knock-down the *Gper1* in CCK^+ neurons, AAV2/9-CMV-DIO-(EGFP-U6)-shRNA (GPR30)-WPRE-pA (5×10^{12} v.g./mL) or AAV2/9-CMV-DIO-(EGFP-U6)-shRNA (Scramble)-WPRE-pA (5×10^{12} v.g./mL) was injected into the lumbar SDH of *CCK-Cre* mice. For visualization of the CCK+ neurons, AAV2/9-CMV-DIO-EGFP-WPRE-pA (5.2×10^{12} v.g./mL) was injected into the lumbar SDH of *CCK-Cre* mice. For anterograde tracing of S1 cortex projections, AAV2/9-hSyn-EGFP-WPRE (1×10^{13} v.g./mL) was in injected into the S1 cortex of wild type mice. For visualization of the S1-SDH post-synaptic neurons,

AAV2/1-hSyn-CRE-WPRE-pA (1×10^{13} v.g./mL) was injected into the S1 cortex and AAV2/9-EF1α-DIO-mCherry-WPRE-pA (1×10^{13} v.g./mL) was injected into the lumbar SDH in wild type mice. For visualization of CCK^+ post-synaptic neurons of S1-SDH projections, AAV2/1- EF1α-FLP-WPRE-pA (1×10^{13} v.g./mL) was injected into the S1 cortex and AAV2/8-hSyn-Con/Fon-EYFP-WPRE-pA (2×10^{12} v.g./mL) was injected into the lumbar SDH of *CCK-Cre* mice. For chemogenetic manipulation of S1-SDH post-synaptic neurons, AAV2/1-hSyn-CRE-WPRE-pA (1×10^{13} v.g./mL) was injected into the S1 cortex, while AAV2/9-hSyn-DIO-hM3Dq (Gq)-mCherry (3.3×10^{13} v.g./mL; dilution: 1:5) or AAV2/9-hSyn-DIO-hM4Di (Gi)-mCherry (3.3×10^{13} v.g./mL; dilution: 1:5) or AAV2/9-hSyn-DIO-mCherry (3×10^{13} v.g./mL; dilution: 1:5) was injected into the lumbar SDH in wild type mice. All viruss mentioned above were purchased from BrainVTA (Wuhan, China). For visualization of the localization of excitatory interneurons in the SDH, AAV2/9-hSyn-mCaMkIIa-mCherry-WPRE-pA (1×10^{13} v.g./mL; Taitool Bioscience, Shanghai, China) was injected into the lumbar SDH of wild type mice.

Chronic constriction injury (CCI)

The CCI-induced neuropathic pain model was employed as previously documented[2]. Mice were lightly anesthetized via inhaled 1.5% Isoflurane. An incision was made on the skin of each mouse, exposing the sciatic nerve. Four ligations with 6-0 chromic silk were loosely tied around the sciatic nerve. Nerve constriction should be minimal until a brief twitch can be observed. In sham mice, the sciatic nerve was exposed without ligation. The animal was allowed to recover from surgery for 2 weeks before behavioral testing.

Behavioral test

Punctate mechanical stimuli (von Frey filaments): Mice were habituated to opaque cage (7.5×15×15 cm) for 1 hour the day before and 30min immediately prior to testing. Testing was performed using a series of von Frey filaments using the Dixon's Up-down method[57], beginning with the 0.16 g filament. The 50% paw withdrawal threshold was determined for each mouse on one hind paws. Each filament was gently applied to the plantar surface of the hind paw for 5 seconds or until a response such as a sharp withdraw, shaking or licking of the limb was observed. Between individual measurement, filaments were applied at least 3 minutes after the mice had returned to their initial resting state.

Dynamic mechanical stimuli (Brush): Each mouse was habituated in an opaque cage (7.5×15×15 cm) for 1 hour the day before and 30 minutes immediately prior to testing. The plantar hind paw was stimulated by light stroking from heel to toe with a paintbrush. A positive response was recorded if the animal lifting, shaking or licking the limb. The application was repeated 10 times with a 3 minutes interval between each stimulation.

Plantar heat test (Hargreaves Method): Mice were placed in an acrylic chamber on a glass table and allowed to acclimate to the test chamber for 1hour the day before and 30 minutes immediately prior to testing. The thermal paw withdrawal latency was assessed using the plantar test (Ugo Basile Biological Research Apparatus, Gemonio, Italy). While the mouse was in a motionless state, a radiant heat source, which was maintained at 40 W, was applied to the plantar surface of the mouse's paw through the glass plate. The paw withdrawal latency was defined as the time to withdrawal of the hind paw from the heat source, and 15 seconds was used as the cut-off to avoid injury.

Real-time place escape/avoidance test (RT-PEA)

Each mouse was habituated in the test room for 1 hour the day before and 30 minutes immediately prior to testing. The Real-time place escape/avoidance chamber (50×28×32 cm; made with plastic plates that had distinct color with another) was placed on the mesh floor. The tested mouse was placed in a two-chamber box and allowed to explore both chambers without any stimulation (pre-stimulation, 10 minutes); mechanical simulation by 0.16 g von Frey filament was intermittently delivered whenever the mouse entered or stayed in the preferred chamber, as shown in the pre-stimulation stage (stimulation,

10 minutes); the mouse then freely explored the box without any stimulation (post-stimulation, 10 minutes). The mouse's movements and time stay in preferred chamber were recorded via an ANY-Maze system.

Immunohistochemistry

Mice were deeply anesthetized with 1% pentobarbital sodium solution and then perfused with phosphate-buffered saline (PBS) followed by pre-cooled 4% paraformaldehyde fix solution (PFA). For c-Fos staining, Von Frey filament with the same force (0.16 g) representing light mechanical stimulation was applied to the right hind paw of each group every 30 s for 20 min. Then animals were then perfused with PBS and 4% PFA ninety minutes after Von Frey filament stimulation. Tissue were harvested and post-fixed in PFA at 4℃ over night before being dehydrated in 30% sucrose for 2days. Tissues were embedded in Optimal Cutting temperature (OCT) and then cut into 10-30 μm sections placed directly onto slides. Tissue slices were blocked at room temperature for an hour with block solution containing 10% normal donkey serum (NDS), 1% bovine serum albumin BSA and 0.3% triton X-100 in PBS (PBS-T), and then incubated with primary antibodies diluted in 1% NDS, 1% BSA in PBS-T

at 4℃ overnight. Sections were washed in PBS and incubated with secondary antibodies at room temperature for 1-2 hours. Slices were washed and covered with Fluoromount-G containing DAPI. All images were taken with an Olympus FV1000 confocal microscope. Antibodies used were as follows: anti-c-Fos (1:1000, guinea pig, Oasis Biofarm, Hangzhou, China), anti-GPR30 (1:500, rabbit, Alomone Labs, Isreal) , anti-IBA1 (1:1000, goat, Novusbio, USA), anti-GFAP (1:1000, mouse, Cell Signaling Technology, USA), IB4-FITC (1:1000, Thermofisher, USA), Nissl (1:500, Thermofisher, USA), goat anti-guinea pig IgG-488 (1:500, Oasis Biofarm, Hangzhou, China), donkey anti-rabbit IgG-488 (1:500, Thermofisher, USA), donkey anti-rabbit IgG-555 (1:500, Thermofisher, USA), donkey anti-mouse IgG-488 (1:500, Thermofisher, USA), donkey anti-goat IgG-488 (1:500, Abcam, USA).

***In Situ* Hybridization**

In situ hybridization was performed according to the manufacturer's instructions from RNAscope® Multiplex Fluorescent Reagent Kit v2 (Advanced Cell diagnostics, USA) with custom-designed probe for *CCK* (Mm-CCK-C1, Advanced Cell diagnostics, USA). According to the protocols, coronal lumbar spinal sections (10 μm) collected and used for fluorescence in situ hybridization to detect CCK^{+} neurons. The slice used to stain RFP primary antibody and *CCK* probewere taken from the -80 °C refrigerator and immediately incubated with pre-cooled 4% PFA for 15 minutes, followed by gradient dehydration (50% ethanol, 70% ethanol, 100% ethanol and 100% ethanol, 5 min for each gradient). The slides were then incubated with RNAscope® hydrogen peroxide at room temperature for 10 minutes, rinsed with distilled water and PBS. Anti-RFP primary antibody (1:1000, rabbit, Rockland,

USA) prepared with co-detection diluent (323180, Advanced Cell Diagnostics) was then added to the slices and incubated overnight at 4 °C for subsequent in situ hybridization staining.

Real-time PCR

Mice lumbar spinal cords were collected on day 4 after CFA and on day 14 after CCI. Tissues were rapidly collected, frozen in liquid nitrogen and stored at -80°C. RNA was extracted with standard procedures using FastPure Cell/Tissue Total RNA Isolation Kit V2 (Vazyme, Nanjing, China). 500ng of total RNA from each sample was reverse-transcribed with HiScript III RT SuperMix for qPCR (+gDNA wiper) (Vazyme, Nanjing, China). Expression of each mRNA was quantified using ChamQ Universal SYBR qPCR Master Mix (Vazyme, Nanjing, China). The sequences of quantitative PCR primers were as follows: *Gper1*: F: CCTCTGCTACTCCCTCATCG, R: ACTATGTGGCCTGTCAAGGG; GAPDH: F: AAGAAGGTGGTGAAGCAGGCATC, R: CGGCATCGAAGGTGGAAGATG.

Spinal slice preparation and whole-cell recording

Spinal slices were prepared as previously described[58]. Mice (6-8-week-old, 2 weeks after CCI surgery) were anesthetized with 1% pentobarbital sodium solution and perfused with ice-cold oxygenated (95% O_2 and 5% CO_2) cutting artificial cerebrospinal fluid (ACSF, in mM: 100 sucrose, 63 NaCl, 2.5 KCl, 1.2 NaH_2PO_4, 1.2 $MgCl_2$, 25 glucose, and 25 $NaHCO_3$), and the spinal cord was rapidly removed. Transverse spinal cord slices (300 μm, L4 to L6 segment) were prepared using a vibratome (VT1200S, Leica, Germany) and incubated in oxygenated NMDG-ACSF (in mM: 93 NMDG, 2.5 KCl, 1.2 NaH_2PO4, 30 $NaHCO_3$, 20 HEPES, 25 Glucose, 5 Na ascorbate, 2 thiourea, 3 Na pyruvate, 10 $MgSO_4$ and 0.5 $CaCl_2$, and adjusted to

pH 7.4 with HCl) at 34 °C for 15 min. The slices were then transferred to normal ACSF (in mM: 125 NaCl, 2.5 KCl, 1.25 NaH_2PO_4, 1.2 $MgCl_2$, 2.5 $CaCl_2$, 25 glucose, and 11 $NaHCO_3$) at 34 °C for 1h and maintained at room temperature before recording. The slices were transferred to a recording chamber perfused with normal ACSF saturated with 95% O_2 and 5% CO_2.

Whole-cell patch- clamp recordings were performed using a Heka EPC 10 amplifier (Heka Elektronik). Borosilicate glass pipettes with the resistance of 3-5 MΩ were pulled using a horizontal pipette puller (P97, Sutter instruments, USA). The pipettes were filled with cesium-based intracellular fluid (in mM: 100 $CsCH_3SO_3$, 20 KCl, 10 HEPES, 4 Mg-ATP, 0.3 Tris-GTP, 7 $Tris_2$-Phosphocreatine, 3 QX-314; pH 7.3, 285–290 mOsm). Targeted whole-cell recordings were made from EGFP expressing neurons in slices taken from *CCK-Cre* mice with virus injection. For spontaneous excitatory post synaptic currents (sEPSCs) recording, the membrane potential was held at -70 mV, and for spontaneous inhibitory post synaptic currents (sIPSCs) recording, the membrane potential was held at +10 mV. Then sEPSCs and sIPSCs were analyzed using MiniAnalysis software (Synaptosoft).

To record AMPA-mediated EPSCs, an electrode placed in the deep laminae of SDH were stimulated at every 15s, and the CCK^+ neurons were voltage clamped at -70 mV. Meanwhile, the spinal slices were incubated with ACSF containing APV (100 μM) to block NMDA receptors and bicuculline (20 μM) and strychnine (0.5 μM) to block inhibitory synaptic events. AMPAR-mediated EPSCs were recorded for 15 consecutive responses after stable baseline before and after G-1 application (0.1 μM) to compare to effect of G-1 on AMPAR-mediated EPSCs.

Statistical analyses

All experiments were randomized. Animals were randomly chosen from multiple cages. For behavior experiments, measurements were taken blinded to condition. All data are reported as mean ± SEM. The required sample sizes were estimated on the basis of our past experience. Statistical analysis was performed using GraphPad Prism V6. Normal distribution was performed using SPSS V20. For all experiments, $P<0.05$ was considered to be statistically significant.

Acknowledgements

This work was supported by the National Natural Science Foundation of China grants (82371220) and 4+X Clinical Research Project of Women's Hospital, School of Medicine, Zhejiang University (ZDFY2022-4XA102). This work was also supported by the Fundamental Research Funds for the Central Universities(2023ZFJH01-01 ,2024ZFJH01-01, and 226-2022-00227). We also thank Sanhua Fang from the Core Facilities, Zhejiang University School of Medicine for their excellent technical assistant.

Author contributions

C.X.Z., and X.Z.Z. conceived the study. C.Q., W.H., X.S.L., X.J.Q, X.L.H., L.H, Z.F.F, conducted the experiments and collected data. C.Q., W.H., and X.S.L. analyzed the data. Y.Y. and Z.H.H. draw the graphic abstract. D.A.G., X.F., Z.W.X., S.L.H., X.Q., W.L.Y and J.C.C. assisted with animal maintenance and provided reagents. C.Q., X.Z.Z. and C.X.Z. wrote the paper.

Conflict of Interest

The authors declare that they have no competing interests.

Data availability

The data that support the findings of this study are available on request from the corresponding author.

Reference

1. Ghazisaeidi, S., Muley, M.M., and Salter, M.W. (2023). Neuropathic Pain: Mechanisms, Sex Differences, and Potential Therapies for a Global Problem. Annu Rev Pharmacol Toxicol *63*, 565-583. 10.1146/annurev-pharmtox-051421-112259.
2. Xia, L.P., Luo, H., Ma, Q., Xie, Y.K., Li, W., Hu, H., and Xu, Z.Z. (2021). GPR151 in nociceptors modulates neuropathic pain via regulating P2X3 function and microglial activation. Brain *144*, 3405-3420. 10.1093/brain/awab245.
3. Cohen, S.P., Vase, L., and Hooten, W.M. (2021). Chronic pain: an update on burden, best practices, and new advances. Lancet *397*, 2082-2097. 10.1016/S0140-6736(21)00393-7.
4. Bannister, K., Sachau, J., Baron, R., and Dickenson, A.H. (2020). Neuropathic Pain: Mechanism-Based Therapeutics. Annu Rev Pharmacol Toxicol *60*, 257-274. 10.1146/annurev-pharmtox-010818-021524.
5. Finnerup, N.B., Kuner, R., and Jensen, T.S. (2021). Neuropathic Pain: From Mechanisms to Treatment. Physiol Rev *101*, 259-301. 10.1152/physrev.00045.2019.
6. Lolignier, S., Eijkelkamp, N., and Wood, J.N. (2015). Mechanical allodynia. Pflugers Arch *467*, 133-139. 10.1007/s00424-014-1532-0.
7. Cheng, L., Duan, B., Huang, T., Zhang, Y., Chen, Y., Britz, O., Garcia-Campmany, L., Ren, X., Vong, L., Lowell, B.B., et al. (2017). Identification of spinal circuits involved in touch-evoked dynamic mechanical pain. Nat Neurosci *20*, 804-814. 10.1038/nn.4549.
8. Ossipov, M.H., Lai, J., Malan, T.P., Jr., and Porreca, F. (2000). Spinal and supraspinal mechanisms of neuropathic pain. Ann N Y Acad Sci *909*, 12-24.

589 10.1111/j.1749-6632.2000.tb06673.x.

590 9. Seal, C.P.a.R.P. (2016). Neural circuits for pain: Recent advances and current views.
591 Science *354*, 578-584. doi: 10.1126/science.aaf8933.

592 10. Peirs, C., Williams, S.G., Zhao, X., Arokiaraj, C.M., Ferreira, D.W., Noh, M.C., Smith,
593 K.M., Halder, P., Corrigan, K.A., Gedeon, J.Y., et al. (2021). Mechanical Allodynia
594 Circuitry in the Dorsal Horn Is Defined by the Nature of the Injury. Neuron *109*, 73-90
595 e77. 10.1016/j.neuron.2020.10.027.

596 11. Abraira, V.E., Kuehn, E.D., Chirila, A.M., Springel, M.W., Toliver, A.A., Zimmerman,
597 A.L., Orefice, L.L., Boyle, K.A., Bai, L., Song, B.J., et al. (2017). The Cellular and
598 Synaptic Architecture of the Mechanosensory Dorsal Horn. Cell *168*, 295-310 e219.
599 10.1016/j.cell.2016.12.010.

600 12. Wang, H., Chen, W., Dong, Z., Xing, G., Cui, W., Yao, L., Zou, W.J., Robinson, H.L.,
601 Bian, Y., Liu, Z., et al. (2022). A novel spinal neuron connection for heat sensation.
602 Neuron *110*, 2315-2333 e2316. 10.1016/j.neuron.2022.04.021.

603 13. Liu, Y., Latremoliere, A., Li, X., Zhang, Z., Chen, M., Wang, X., Fang, C., Zhu, J.,
604 Alexandre, C., Gao, Z., et al. (2018). Touch and tactile neuropathic pain sensitivity are
605 set by corticospinal projections. Nature *561*, 547-550. 10.1038/s41586-018-0515-2.

606 14. Li, L.H., Ling, D.D., Lin, H., Wang, Z.C., Sun, Z.R., Zhang, Y.Q., Yang, L., Zhang, J.,
607 and Cao, H. (2023). Ovariectomy induces hyperalgesia accompanied by upregulated
608 estrogen receptor alpha and protein kinase B in the rat spinal cord. Physiol Behav *271*,
609 114342. 10.1016/j.physbeh.2023.114342.

610 15. Lee, J., Chung, S., Hwang, M., Kwon, Y., Han, S.H., and Lee, S.J. (2023). Estrogen

611 Mediates the Sexual Dimorphism of GT1b-Induced Central Pain Sensitization. Cells
612 *12*. 10.3390/cells12050808.
613 16. Xu, Z., Xie, W., Feng, Y., Wang, Y., Li, X., Liu, J., Xiong, Y., He, Y., Chen, L., Liu, G.,
614 and Wu, Q. (2022). Positive interaction between GPER and beta-alanine in the dorsal
615 root ganglion uncovers potential mechanisms: mediating continuous neuronal
616 sensitization and neuroinflammation responses in neuropathic pain. J
617 Neuroinflammation *19*, 164. 10.1186/s12974-022-02524-9.
618 17. Vannuccini, S., Clemenza, S., Rossi, M., and Petraglia, F. (2022). Hormonal
619 treatments for endometriosis: The endocrine background. Rev Endocr Metab Disord
620 *23*, 333-355. 10.1007/s11154-021-09666-w.
621 18. Sharp, J.L., Pearson, T., and Smith, M.A. (2022). Sex differences in opioid receptor
622 mediated effects: Role of androgens. Neurosci Biobehav Rev *134*, 104522.
623 10.1016/j.neubiorev.2022.104522.
624 19. Tramullas, M., Collins, J.M., Fitzgerald, P., Dinan, T.G., SM, O.M., and Cryan, J.F.
625 (2021). Estrous cycle and ovariectomy-induced changes in visceral pain are
626 microbiota-dependent. iScience *24*, 102850. 10.1016/j.isci.2021.102850.
627 20. Pang, H., Chen, S., Klyne, D.M., Harrich, D., Ding, W., Yang, S., and Han, F.Y. (2023).
628 Low back pain and osteoarthritis pain: a perspective of estrogen. Bone Res *11*, 42.
629 10.1038/s41413-023-00280-x.
630 21. Duan, L.L., Qiu, X.Y., Wei, S.Q., Su, H.Y., Bai, F.R., Traub, R.J., Zhou, Q., and Cao,
631 D.Y. (2021). Spinal CCK contributes to somatic hyperalgesia induced by orofacial
632 inflammation combined with stress in adult female rats. Eur J Pharmacol *913*, 174619.

633 10.1016/j.ejphar.2021.174619.

634 22. Arnal, J.F., Lenfant, F., Metivier, R., Flouriot, G., Henrion, D., Adlanmerini, M.,
635 Fontaine, C., Gourdy, P., Chambon, P., Katzenellenbogen, B., and Katzenellenbogen,
636 J. (2017). Membrane and Nuclear Estrogen Receptor Alpha Actions: From Tissue
637 Specificity to Medical Implications. Physiol Rev *97*, 1045-1087.
638 10.1152/physrev.00024.2016.

639 23. Chen, Q., Zhang, W., Sadana, N., and Chen, X. (2021). Estrogen receptors in pain
640 modulation: cellular signaling. Biol Sex Differ *12*, 22. 10.1186/s13293-021-00364-5.

641 24. Jiao, Y., Gao, P., Dong, L., Ding, X., Meng, Y., Qian, J., Gao, T., Wang, R., Jiang, T.,
642 Zhang, Y., et al. (2023). Molecular identification of bulbospinal ON neurons by GPER,
643 which drives pain and morphine tolerance. J Clin Invest *133*. 10.1172/JCI154588.

644 25. Jie Luo, X.H., Yali Li, Yang Li, Xueqin Xu, Yan Gao, Ruoshi Shi, Wanjun Yao, Juying
645 Liu, Changbin Ke (2016). GPR30 disrupts the balance of GABAergic and
646 glutamatergic transmission in the spinal cord driving to the development of bone
647 cancer pain. Oncotarget *7*, 73462-73472. 10.18632/oncotarget.11867.

648 26. Takanami, K., Sakamoto, H., Matsuda, K., Hosokawa, K., Nishi, M., Prossnitz, E.R.,
649 and Kawata, M. (2010). Expression of G protein-coupled receptor 30 in the spinal
650 somatosensory system. Brain Res *1310*, 17-28. 10.1016/j.brainres.2009.11.004.

651 27. Qi, L., Lin, S.H., and Ma, Q. (2023). Spinal VGLUT3 lineage neurons drive visceral
652 mechanical allodynia but not sensitized visceromotor reflexes. Neuron *111*, 669-681
653 e665. 10.1016/j.neuron.2022.12.003.

654 28. Stephanie C Koch, D.A.a.M.G. (2018). Spinal Circuits for Touch, Pain, and Itch.

655 Annual Review of Physiology. 10.1146/annurev-physiol-.

656 29. Zhang, Y., Xiao, X., Zhang, X.M., Zhao, Z.Q., and Zhang, Y.Q. (2012). Estrogen
657 facilitates spinal cord synaptic transmission via membrane-bound estrogen receptors:
658 implications for pain hypersensitivity. J Biol Chem *287*, 33268-33281.
659 10.1074/jbc.M112.368142.

660 30. Cai, B., Wu, D., Xie, H., Chen, Y., Wang, H., Jin, S., Song, Y., Li, A., Huang, S., Wang,
661 S., et al. (2023). A direct spino-cortical circuit bypassing the thalamus modulates
662 nociception. Cell Res *33*, 775-789. 10.1038/s41422-023-00832-0.

663 31. Zhang, W., Wu, H., Xu, Q., Chen, S., Sun, L., Jiao, C., Wang, L., Fu, F., Feng, Y.,
664 Qian, X., and Chen, X. (2020). Estrogen modulation of pain perception with a novel
665 17beta-estradiol pretreatment regime in ovariectomized rats. Biol Sex Differ *11*, 2.
666 10.1186/s13293-019-0271-5.

667 32. Deng, C., Gu, Y.J., Zhang, H., and Zhang, J. (2017). Estrogen affects neuropathic
668 pain through upregulating N-methyl-D-aspartate acid receptor 1 expression in the
669 dorsal root ganglion of rats. Neural Regen Res *12*, 464-469.
670 10.4103/1673-5374.202925.

671 33. Wang, J., Wang, S., Fang, Z., Zhao, J., Zhang, G., Guo, Y., Wang, Q., Jiang, Z.,
672 Zhong, H., and Hou, W. (2024). Estrogen receptor GPR30 in the anterior cingulate
673 cortex mediates exacerbated neuropathic pain in ovariectomized mice. Brain Res,
674 148798. 10.1016/j.brainres.2024.148798.

675 34. Li, J., Gao, P., Zhang, S., Lin, X., Chen, J., Zhang, S., Jiao, Y., Yu, W., Xia, X., and
676 Yang, L. (2024). The G protein-coupled estrogen receptor of the trigeminal ganglion

677 regulates acute and chronic itch in mice. CNS Neurosci Ther *30*, e14367.
678 10.1111/cns.14367.
679 35. Jiang, M., Sun, Y., Lei, Y., Hu, F., Xia, Z., Liu, Y., Ma, Z., and Gu, X. (2020). GPR30
680 receptor promotes preoperative anxiety-induced postoperative hyperalgesia by
681 up-regulating GABA(A)-alpha4beta1delta subunits in periaqueductal gray in female
682 rats. BMC Anesthesiol *20*, 93. 10.1186/s12871-020-01017-7.
683 36. Liu, S.B., Tian, Z., Guo, Y.Y., Zhang, N., Feng, B., and Zhao, M.G. (2015). Activation
684 of GPR30 attenuates chronic pain-related anxiety in ovariectomized mice.
685 Psychoneuroendocrinology *53*, 94-107. 10.1016/j.psyneuen.2014.12.021.
686 37. Tian, Z., Wang, Y., Zhang, N., Guo, Y.Y., Feng, B., Liu, S.B., and Zhao, M.G. (2013).
687 Estrogen receptor GPR30 exerts anxiolytic effects by maintaining the balance
688 between GABAergic and glutamatergic transmission in the basolateral amygdala of
689 ovariectomized mice after stress. Psychoneuroendocrinology *38*, 2218-2233.
690 10.1016/j.psyneuen.2013.04.011.
691 38. An, G., Li, W., Yan, T., and Li, S. (2014). Estrogen rapidly enhances incisional pain of
692 ovariectomized rats primarily through the G protein-coupled estrogen receptor. Int J
693 Mol Sci *15*, 10479-10491. 10.3390/ijms150610479.
694 39. Deliu, E., Brailoiu, G.C., Arterburn, J.B., Oprea, T.I., Benamar, K., Dun, N.J., and
695 Brailoiu, E. (2012). Mechanisms of G protein-coupled estrogen receptor-mediated
696 spinal nociception. J Pain *13*, 742-754. 10.1016/j.jpain.2012.05.011.
697 40. Xiang, H.C., Lin, L.X., Hu, X.F., Zhu, H., Li, H.P., Zhang, R.Y., Hu, L., Liu, W.T., Zhao,
698 Y.L., Shu, Y., et al. (2019). AMPK activation attenuates inflammatory pain through

699 inhibiting NF-kappaB activation and IL-1beta expression. J Neuroinflammation *16*, 34.
700 10.1186/s12974-019-1411-x.
701 41. Mogil, J.S. (2020). Qualitative sex differences in pain processing: emerging evidence
702 of a biased literature. Nat Rev Neurosci *21*, 353-365. 10.1038/s41583-020-0310-6.
703 42. Vacca, V., Marinelli, S., Pieroni, L., Urbani, A., Luvisetto, S., and Pavone, F. (2014).
704 Higher pain perception and lack of recovery from neuropathic pain in females: a
705 behavioural, immunohistochemical, and proteomic investigation on sex-related
706 differences in mice. Pain *155*, 388-402. 10.1016/j.pain.2013.10.027.
707 43. Vacca, V., Marinelli, S., Pieroni, L., Urbani, A., Luvisetto, S., and Pavone, F. (2016).
708 17beta-estradiol counteracts neuropathic pain: a behavioural, immunohistochemical,
709 and proteomic investigation on sex-related differences in mice. Sci Rep *6*, 18980.
710 10.1038/srep18980.
711 44. Zhang, Y., Lu, N., Zhao, Z.Q., and Zhang, Y.Q. (2012). Involvement of estrogen in
712 rapid pain modulation in the rat spinal cord. Neurochem Res *37*, 2697-2705.
713 10.1007/s11064-012-0859-1.
714 45. Swetha E Murthy, M.C.L., Ihab Daou, Kara L Marshall, Frederick Schwaller, Johannes
715 Kühnemund, Allain G Francisco, William T Keenan, Adrienne E Dubin, Gary R Lewin,
716 Ardem Patapoutian (2018). The mechanosensitive ion channel Piezo2 mediates
717 sensitivity to mechanical pain in mice. Science Translational Medicine *10* (*462*),
718 eaat9897.
719 46. Alice Arcourt, S.G.L. (2015). Peripheral and spinal circuits involved in mechanical
720 allodynia. Pain *156*, 220-221. 10.1097/01.j.pain.0000460818.62406.38.

721 47. Cao, B., Scherrer, G., and Chen, L. (2022). Spinal cord retinoic acid receptor signaling
722 gates mechanical hypersensitivity in neuropathic pain. Neuron *110*, 4108-4124 e4106.
723 10.1016/j.neuron.2022.09.027.
724 48. David S Bredt, R.A.N. (2003). AMPA receptor trafficking at excitatory synapses.
725 Neuron *40*, 361-379. 10.1016/s0896-6273(03)00640-8.
726 49. Basbaum, A.I., Bautista, D.M., Scherrer, G., and Julius, D. (2009). Cellular and
727 molecular mechanisms of pain. Cell *139*, 267-284. 10.1016/j.cell.2009.09.028.
728 50. Frank Porreca, M.H.O.a.G.F.G. (2002). Chronic pain and medullary
729 descending facilitation. TRENDS in Neurosciences *25*.
730 51. Shannon E. Burgess, L.R.G., Michael H. Ossipov, T. Philip Malan Jr, Todd W.
731 Vanderah,, and Josephine Lai, a.F.P. (2002). Time-Dependent Descending
732 Facilitation from the Rostral
733 Ventromedial Medulla Maintains, But Does Not Initiate,
734 Neuropathic Pain. The Journal of Neuroscience *22*, 5129–5136.
735 52. L. R. Gardell, T.W.V., S. E. Gardell, R. Wang, M. H. Ossipov, J. Lai, and F. Porreca
736 (2003). Enhanced Evoked Excitatory Transmitter Release in
737 Experimental Neuropathy Requires Descending Facilitation. The Journal of Neuroscience *23*,
738 8370 – 8379.
739 53. Bee, L.A., and Dickenson, A.H. (2007). Rostral ventromedial medulla control of spinal
740 sensory processing in normal and pathophysiological states. Neuroscience *147*,
741 786-793. 10.1016/j.neuroscience.2007.05.004.
742 54. Bannister, K., and Dickenson, A.H. (2017). The plasticity of descending controls in

743 pain: translational probing. J Physiol *595*, 4159-4166. 10.1113/JP274165.

744 55. Lau, B.K., and Vaughan, C.W. (2014). Descending modulation of pain: the GABA
745 disinhibition hypothesis of analgesia. Curr Opin Neurobiol *29*, 159-164.
746 10.1016/j.conb.2014.07.010.

747 56. Wu, Z.H., Shao, H.Y., Fu, Y.Y., Wu, X.B., Cao, D.L., Yan, S.X., Sha, W.L., Gao, Y.J.,
748 and Zhang, Z.J. (2021). Descending Modulation of Spinal Itch Transmission by
749 Primary Somatosensory Cortex. Neurosci Bull *37*, 1345-1350.
750 10.1007/s12264-021-00713-9.

751 57. Dixon, W.J. (1980). EFFICIENT ANALYSIS OF EXPERIMENTAL OBSERVATIONS.
752 Ann Rev Pharmacol Toxicol.

753 58. Winters, B.L., Rawling, T., Vandenberg, R.J., Christie, M.J., Bhola, R.F., and Imlach,
754 W.L. (2018). Activity of novel lipid glycine transporter inhibitors on synaptic signalling
755 in the dorsal horn of the spinal cord. Br J Pharmacol *175*, 2337-2347.
756 10.1111/bph.14189.

757

Figures and Legends

Fig 1

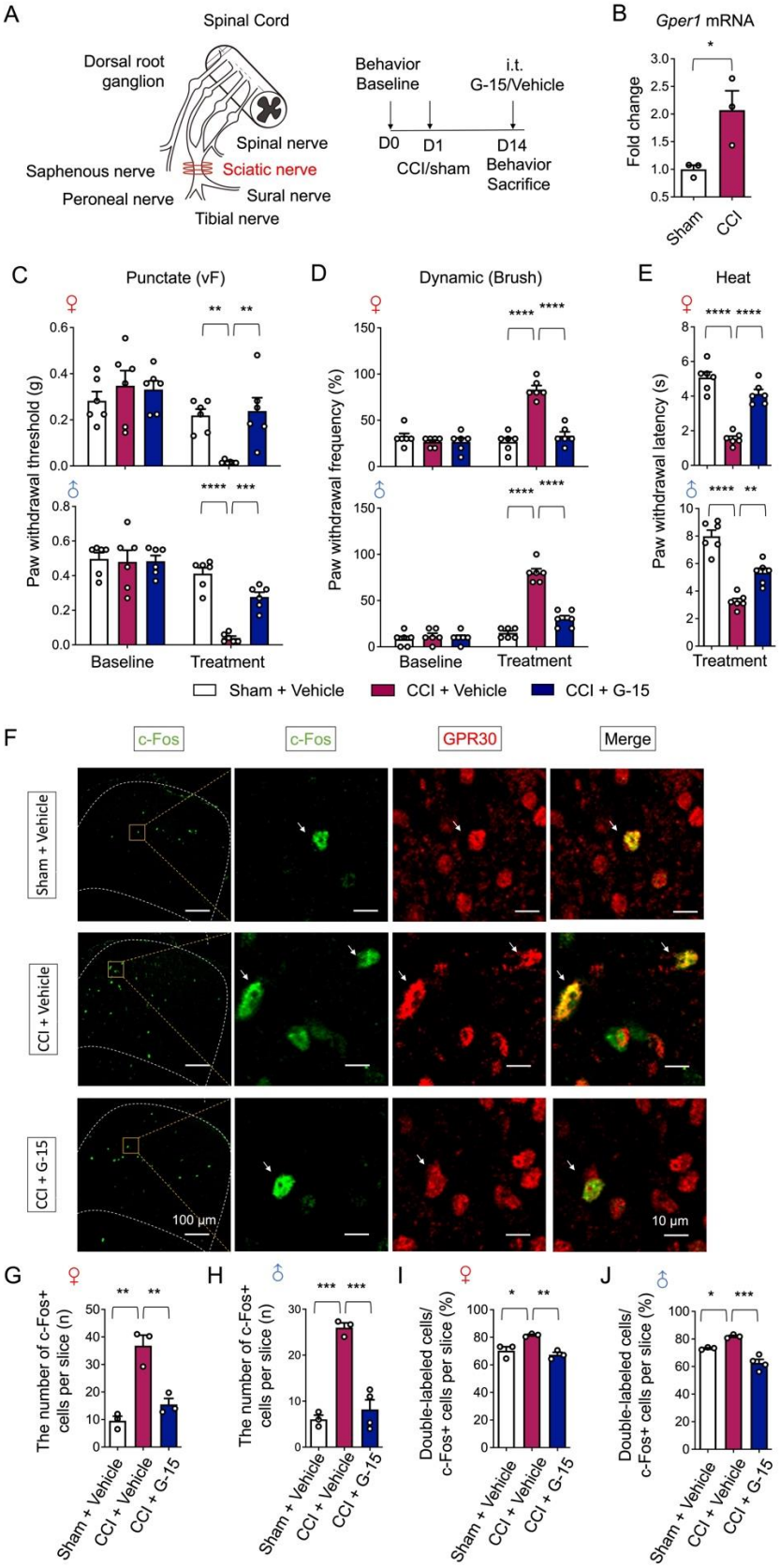

Figure 1 - CCI-induced neuropathic pain and neuronal activation were reversed by spinal inhibition of GPR30.

A Schematic illustration of CCI surgery for induction of neuropathic pain (Left) and diagram showing the timeline of CCI surgery, drug administration and behavioral tests (Right).

B Quantitative PCR analysis of *Gper1* mRNA in SDH from sham and CCI mice (n = 3 mice for each group).

C-E Behavioral tests of basic nociception and 14 days after CCI or sham surgery along with intrathecal injection of antagonist of GPR30 or vehicle in Von Frey tests **(C)**, Brush tests **(D)** and Heat tests **(E)** in mice of both genders (n = 6 mice for each group).

F Immunochemical detection of c-Fos (Green) and GPR30 (Red). Scale bars: 100 μm. Boxed area of images is enlarged on the right. Scale bars: 10 μm. White arrows indicate double-positive cells.

G, H Total number of c-Fos positive neurons in the SDH per section in female mice **(G)** and male mice **(H)** (n = 3-4 mice for each group).

I, J Percentage of c-Fos positive neurons expressing GPR30 in female mice **(I)** and male mice **(J)**. (n = 3-4 mice for each group).

Data information: in **(B)**, $*P < 0.05$ (Unpaired Student's t-test). In **(C, D)**, $**P < 0.01$; $***P < 0.001$; $****P < 0.0001$ (two-way ANOVA with Turkey's multiple comparisons test). In **(E)**, $**P < 0.01$; $****P < 0.0001$ (one-way ANOVA with Turkey's multiple comparisons test). In **(G-J)**, $*P < 0.05$; $**P < 0.01$; $***P < 0.001$ (one-way ANOVA with Turkey's multiple comparisons test). All data are presented as mean ± SEM.

Fig 2

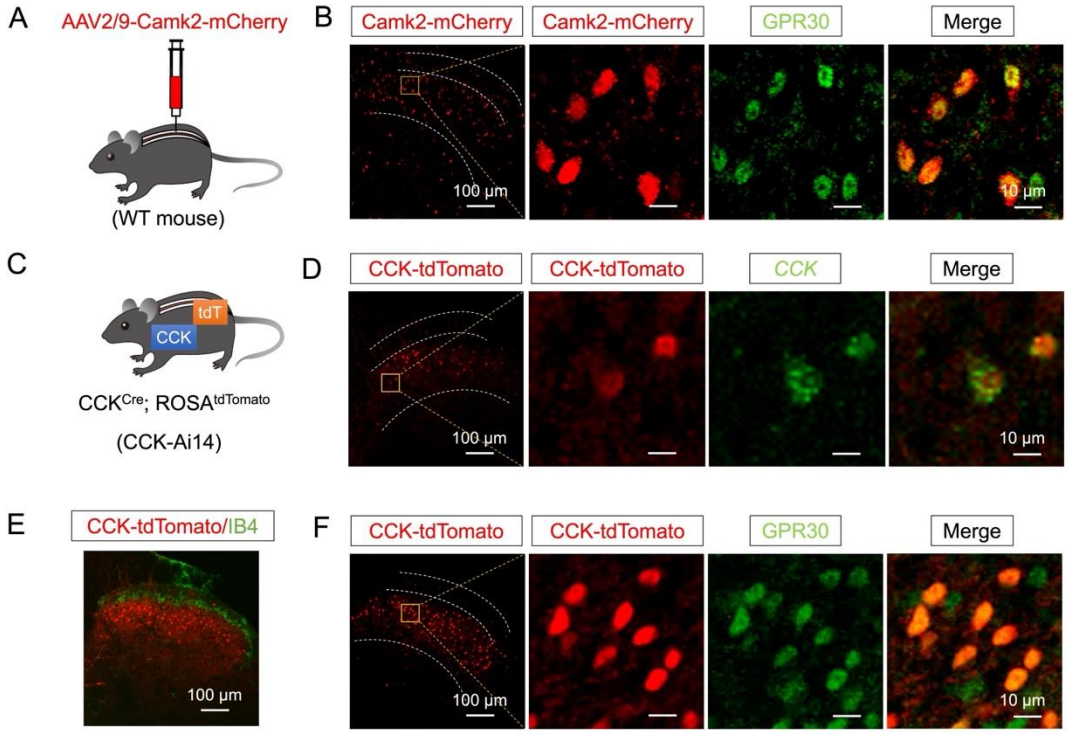

Figure 2 - GPR30 was widely expressed in the CCK$^+$ excitatory interneurons in the SDH.

A Schematic illustration of the strategy to identify the Camk2$^+$ excitatory interneurons in spinal dorsal horn by AAV (left).

B Double staining of Camk2$^+$ mCherry$^+$ neurons (Red) with GPR30 (Green) by immunohistochemistry. Scale bars: 100 μm. Boxed area of images is enlarged on the right. Scale bars: 10 μm.

C CCK^{Cre} mice express tdTomato in a Cre-dependent manner.

D *In situ* hybridization showing *CCK* (Green) with tdTomato (Red) in the SDH. Scale bar: 100 μm. Boxed area of image is enlarged on the right. Scale bars: 10 μm.

E Double staining of tdTomato$^+$ neurons (Red) with IB4 (Green) by immunochemistry. Scale

bars: 100 μm.

F Immunofluorescence in SDH to verify the co-localization of tdTomato^{+} neurons (Red) with GPR30 (Green). Scale bars: 100 μm. Boxed area of images is enlarged on the right. Scale bars: 10 μm.

Fig 3

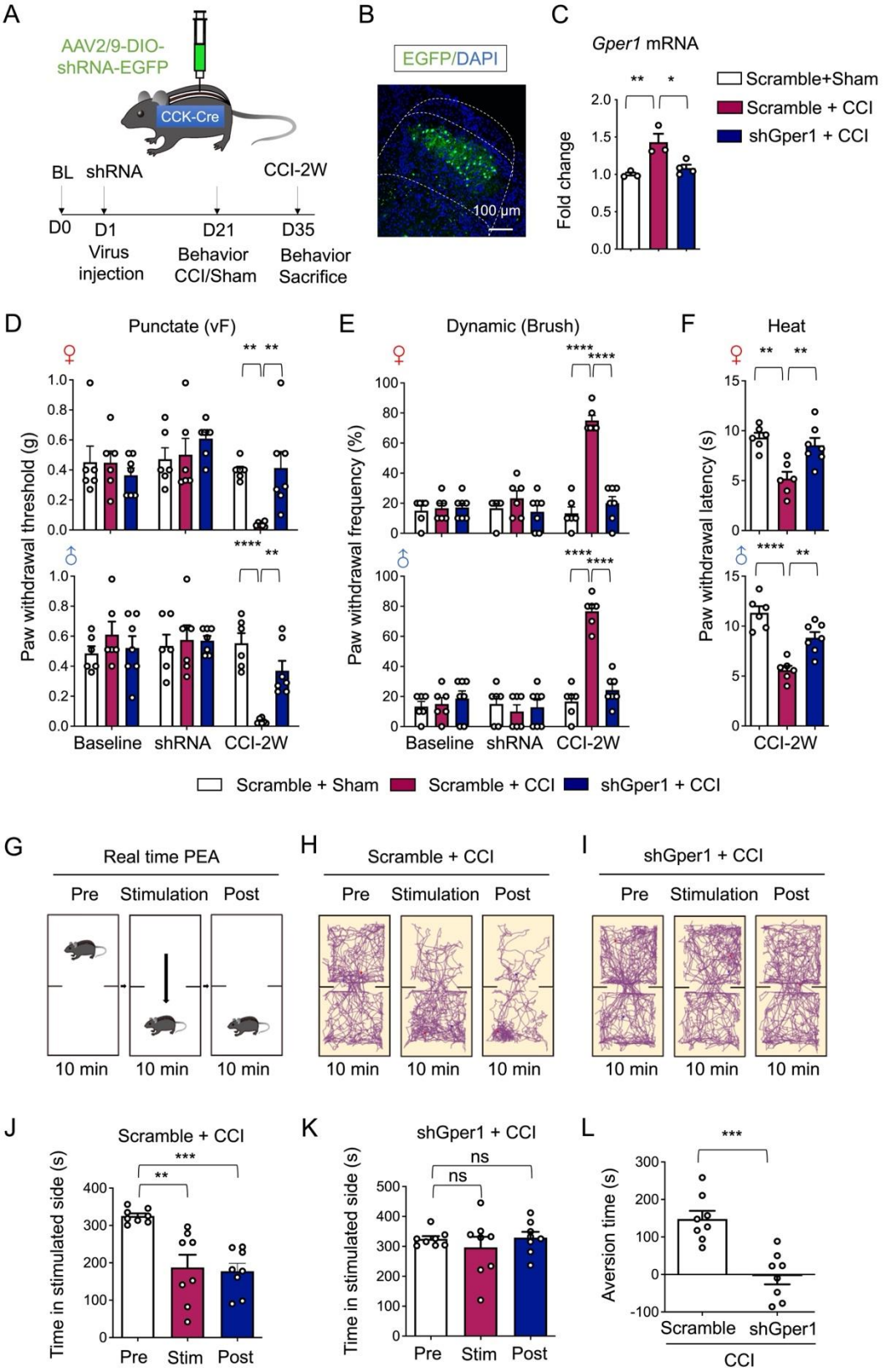
A
AAV2/9-DIO-shRNA-EGFP
CCK-Cre
BL
shRNA
CCI-2W
D0
D1
D21
D35
Virus injection
Behavior CCI/Sham
Behavior Sacrifice
B
EGFP/DAPI
100 μm
C
Gper1 mRNA
Fold change
Scramble+Sham
Scramble + CCI
shGper1 + CCI
D
Punctate (vF)
Paw withdrawal threshold (g)
Baseline
shRNA
CCI-2W
E
Dynamic (Brush)
Paw withdrawal frequency (%)
F
Heat
Paw withdrawal latency (s)
Scramble + Sham
Scramble + CCI
shGper1 + CCI
G
Real time PEA
Pre
Stimulation
Post
10 min
H
Scramble + CCI
I
shGper1 + CCI
J
Scramble + CCI
Time in stimulated side (s)
Pre
Stim
Post
K
shGper1 + CCI
ns
L
Aversion time (s)
Scramble
shGper1
CCI

797

Figure 3 - Knockdown of GPR30 in spinal CCK$^+$ neurons alleviated neuropathic pain in CCI mice.

A Schematic illustration of the strategy to knock down Gper1 in the spinal CCK$^+$ neurons in a Cre-dependent manner (Up) and the diagram showing the timeline of virus injection, CCI surgery and behavioral tests (Down).

B Immunochemical detection of the localization of virus expression (Green). Scale bars: 100 μm.

C Quantitative PCR analysis of *Gper1* mRNA in SDH from sham and CCI mice with intraspinal virus injection (n = 3-4 mice for each group).

D-F Behavioral tests of basic nociception, 21 days after spinal virus injection and 14 days after CCI or sham surgery along with intrathecal injection of antagonist of GPR30 or vehicle in Von Frey tests **(D)**, Brush tests **(E)** and Heat tests **(F)** in mice of both genders (n = 6-7 mice for each group).

G Schematic illustration of real-time place escape/avoidance (PEA) test.

H, I Representative spatial tracking maps showing the location of a Scramble + CCI group mice **(H)** and a shGper1 + CCI group mice **(I)** before, during and after mechanical stimulation of hind paw in the chambers.

J Quantification of time the Scramble + CCI group mice spent in preferred chamber before, during and after stimulation (n = 8 mice).

K Quantification of time the shGper1 + CCI group mice spent in preferred chamber before, during and after stimulation (n = 8 mice).

L Quantification of the aversion time of mice. (time spent in preferred chamber after stimulation minus the time spent before stimulation) (n = 8 mice for each group).

Data information: in **(C)**, *$P < 0.05$; **$P < 0.01$ (one-way ANOVA with Turkey's multiple comparisons test). In **(D, E)**, **$P < 0.01$; ****$P < 0.0001$ (two-way ANOVA with Turkey's multiple comparisons test). In **(F)**, **$P < 0.01$; ****$P < 0.0001$ (one-way ANOVA with Turkey's multiple comparisons test). In **(J, K)**, *$P < 0.05$; **$P < 0.01$; ***$P < 0.001$; ns = not significant. (one-way ANOVA with Turkey's multiple comparisons test). In **(L)**, ***$P < 0.001$ (Unpaired Student's t-test). All data are presented as mean ± SEM.

Fig 4

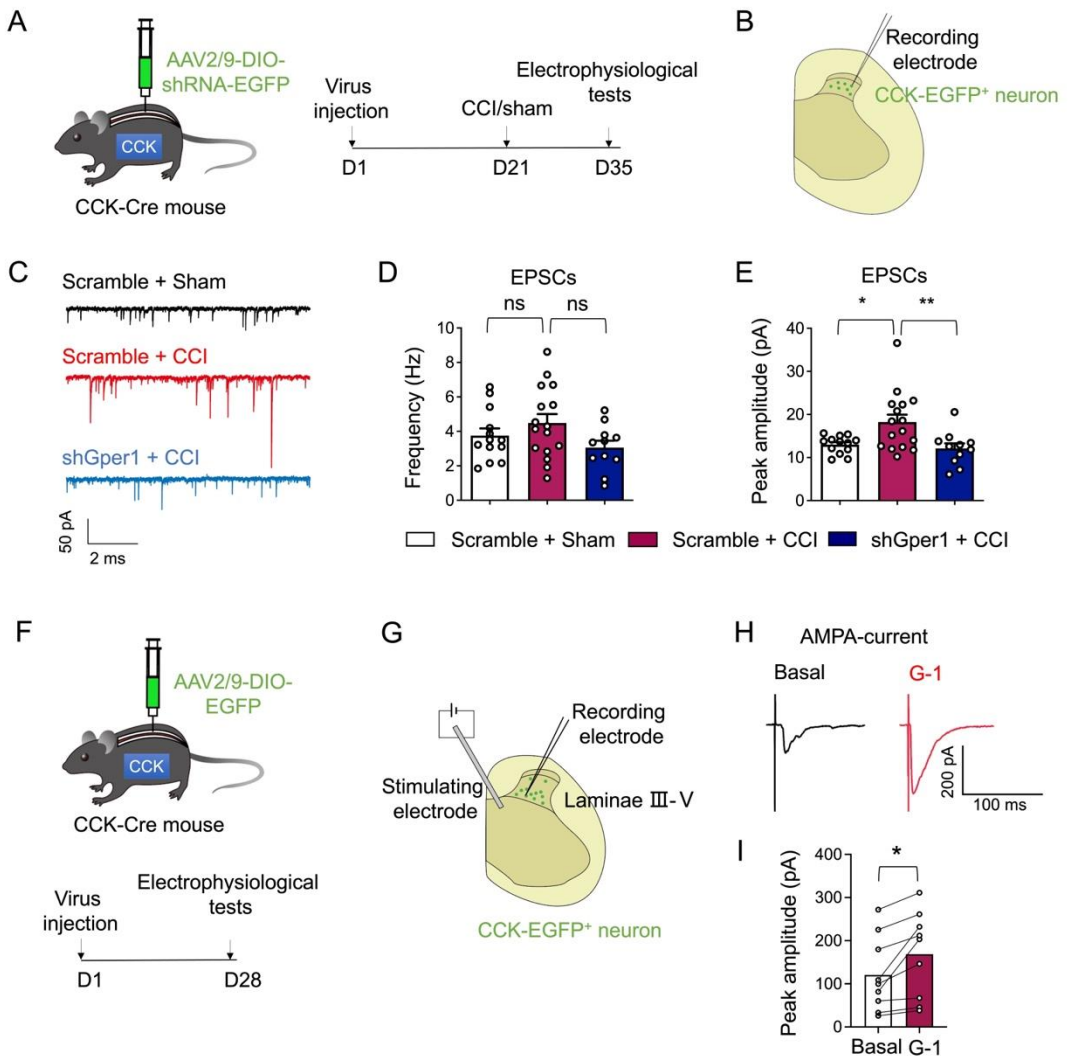

Figure 4 - Knockdown of GPR30 in spinal CCK$^+$ neurons reverse the enhancement of sEPSC in CCI mice

A Schematic illustration of the strategy to knock down Gper1 in the spinal CCK$^+$ neurons in a Cre-dependent manner (Left) and the diagram showing the timeline of virus injection, CCI surgery and electrophysiological tests (Right).

B Schematic illustration of spinal slice electrophysiological recordings from CCK-EGFP neurons located in the deep laminae of SDH.

C Representative spontaneous EPSCs in CCK-EGFP neurons.

D The frequency of spontaneous EPSCs.

E The peak amplitude spontaneous EPSCs (n = 10-16 cells from 5 mice).

F Schematic illustration of the strategy to visualize CCK^+ neurons in a Cre-dependent manner (Up) and the diagram showing the timeline of virus injection and electrophysiological tests (Down).

G Schematic illustration of spinal slice electrophysiological recordings from $CCK\text{-}EGFP^+$ neurons located in the deep laminae of SDH during electric stimulation of the deep laminae of SDH to simulate APMA currents.

H Representative AMPA-current in $CCK\text{-}EGFP^+$ neurons before and after administration of G-1.

I The peak amplitude AMPA currents before and after administration of G-1 (n = 8 cells from 4 mice).

Data information: in **(D, E)**, $*P < 0.05$; $**P < 0.01$; ns = not significant (one-way ANOVA with Turkey's multiple comparisons test). In **(I)**, $*P < 0.05$ (Paired Student's t-test). All data are presented as mean ± SEM.

Fig 5

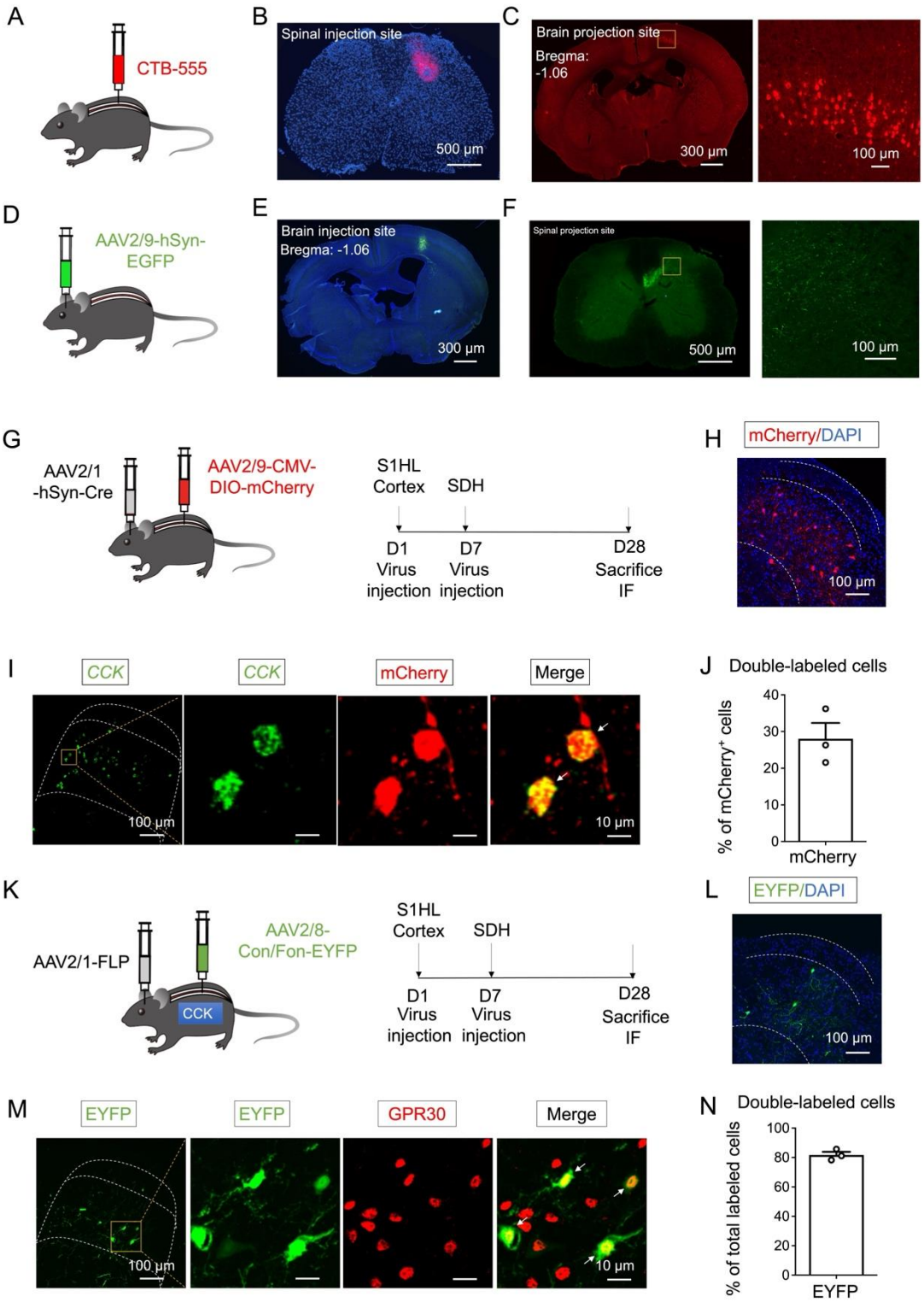

Figure 5 - GPR30 was expressed in the spinal CCK$^+$ neurons receiving direct projection from S1 cortex.

A Schematic illustration of the strategy to retrograde tracing the projections innervating spinal dorsal horn via CTB-555.

B Fluorescence image showing the site of CTB-555 injection in the spinal dorsal horn. Scale bars: 500 μm.

C Coronal brain section showing the location of tdTomato+ neurons in the S1HL cortex. Scale bars: 300 μm. Boxed area of image is enlarged on the right. Scale bars: 100 μm.

D Schematic illustration of the strategy to anterograde tracing the projections from S1HL cortex.

E Coronal brain section showing the site of AAV injection in the S1HL cortex. Scale bars: 300 μm.

F Fluorescence image showing the S1HL-SDH tract terminates in the deep laminae of spinal dorsal horn. Scale bars: 500 μm. Boxed area of image is enlarged on the right. Scale bars: 100 μm.

G Schematic illustration of the strategy for identifying the spinal post-synaptic neurons of S1-SDH projections (Left) and diagram showing the timeline of AAV2/1 injection in the S1HL cortex, AAV2/9 injection in the spinal dorsal horn and immunofluorescence (Right).

H Representative image showing the mCherry^{+} post-synaptic neurons of the S1HL-SDH projections in the deep laminae of SDH. Scale bars: 100 μm.

I *In situ* hybridization showing *CCK* (Green) with RFP (Red) by immunofluorescence in the spinal dorsal horn. Scale bars: 100 μm. Boxed area of image is enlarged on the right. Scale bars: 10 μm. White arrows indicate double-positive cells.

J About 28.13% of RFP^+ post-synaptic neurons of S1HL-SDH projections expressing *CCK* (n = 3 mice).

K Schematic illustration of the strategy for identifying the spinal CCK^+ post-synaptic neurons of S1HL-SDH projections in CCK^{Cre} mice (Left) and diagram showing the timeline of AAV2/1 injection in the S1HL cortex, AAV2/9 injection in the spinal dorsal horn and immunofluorescence (Right).

L Representative image showing the $EGFP^+$ CCK^+ post-synaptic neurons of the S1-SDH projections in the spinal dorsal horn with DAPI. Scale bars: 100 μm.

M Double staining of $EGFP^+$ neurons with GPR30 by immunohistochemistry. Scale bars: 100 μm. Boxed area of image is enlarged on the right. Scale bars: 10 μm.

N About 81.7% of CCK+ post-synaptic neurons of S1HL-SDH projections expressing GPR30 (n = 3 mice).

Data information: in **(J, N)**, data are presented as mean ± SEM.

Fig 6

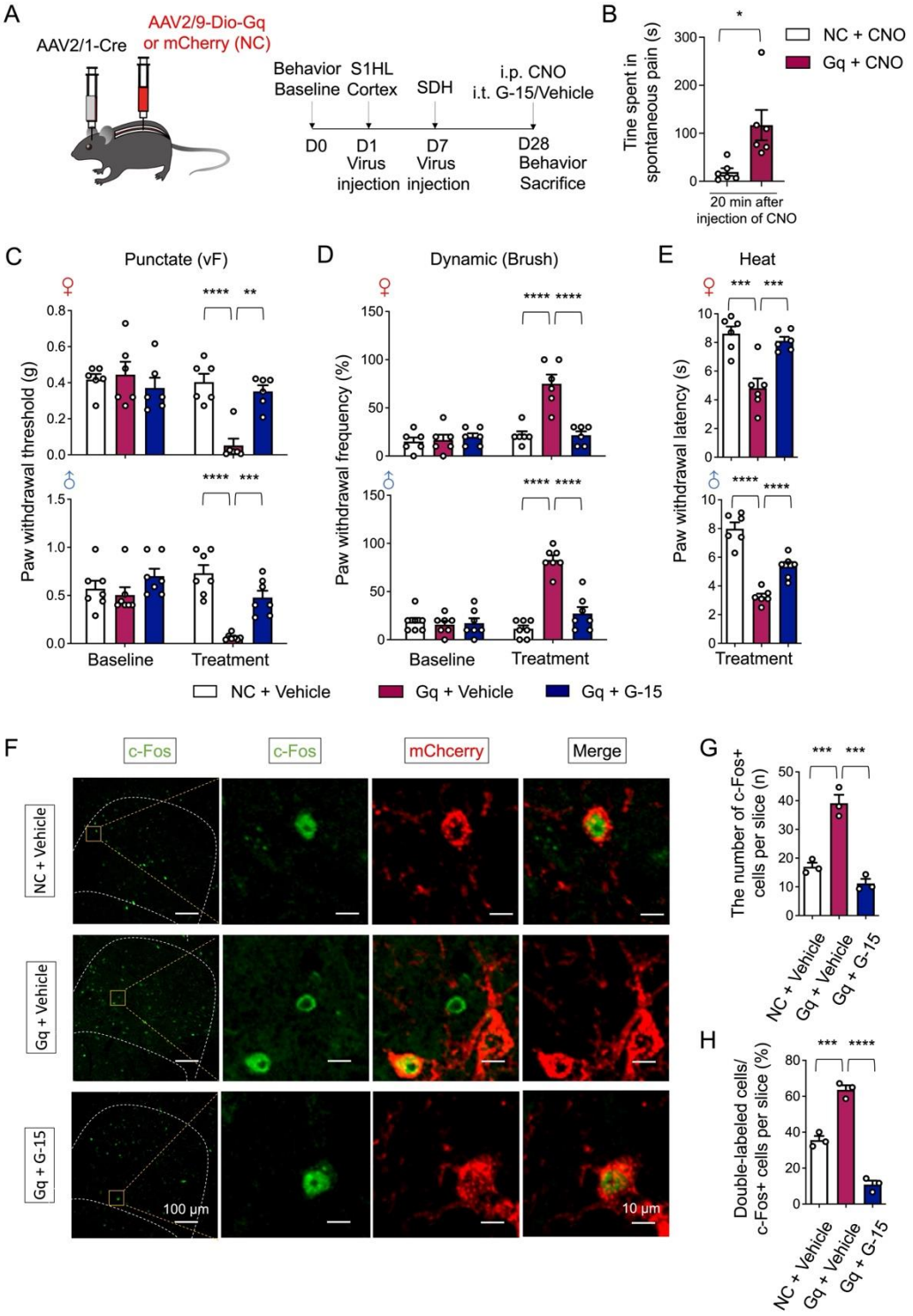

Figure 6 - Chemogenetic activation of S1-SDH post-synaptic neurons mimicked neuropathic pain symptoms, which were reversed by spinal inhibition of GPR30.

A Schematic illustration of the strategy for identifying the post-synaptic neurons of

S1HL-SDH projections in SDH (Left) and diagram showing the timeline of AAV2/1 injection in the S1HL cortex, AAV2/9 injection in the spinal dorsal horn and behavioral tests (Right).

B Spontaneous pain induced by intraperitoneal injection of CNO within 20 min (n = 6 mice for each group).

C-E Behavioral tests of basic nociception, 28 days after brain virus injection along with intraperitoneal injection of CNO and intrathecal injection of antagonist of GPR30 or vehicle in Von Frey tests **(C)**, Brush tests **(D)** and Heat tests **(E)** in mice of both genders (n = 6 mice for each group).

F Immunochemical detection of c-Fos (Green) and m-Cherry+ post-synaptic neurons (Red). Scale bars: 100 μm. Boxed area of images is enlarged on the right. Scale bars: 10 μm.

G Total number of c-Fos positive neurons in the SDH per section (n = 3 mice for each group).

H Percentage of c-Fos positive neurons expressed in m-Cherry (n = 3 mice for each group).

Data information: in **(B)**, *$P < 0.05$ (Unpaired Student's t-test). In **(C, D)**, **$P < 0.01$; ***$P < 0.001$; ****$P < 0.0001$ (two-way ANOVA with Turkey's multiple comparisons test). In **(E)**, ***$P < 0.001$; ****$P < 0.0001$ (one-way ANOVA with Turkey's multiple comparisons test). In **(G, H)**, ***$P < 0.001$; ****$P < 0.0001$. (one-way ANOVA with Turkey's multiple comparisons test). All data are presented as mean ± SEM.

Fig 7

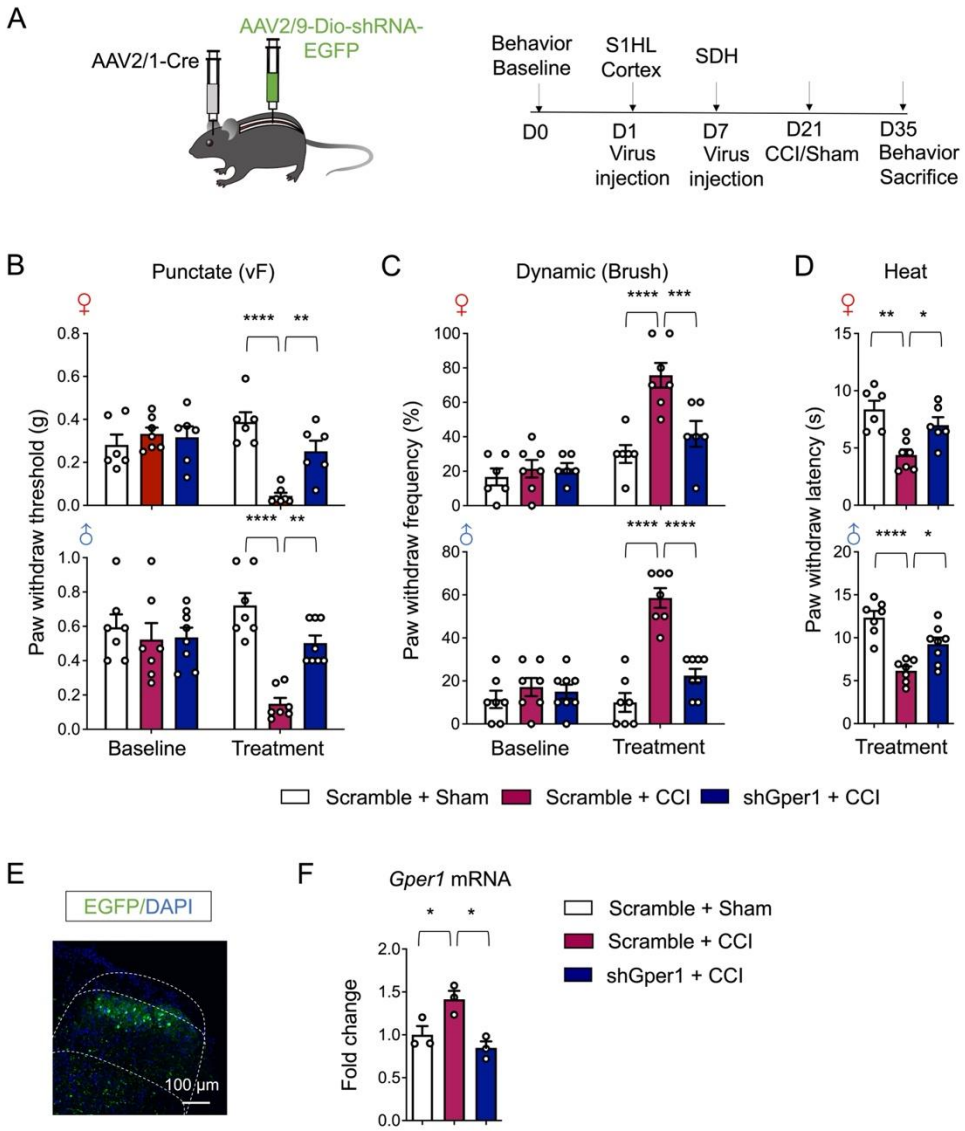

Figure 7 - CCI-induced neuropathic pain was attenuated by knock-down of GPR30 in S1-SDH post-synaptic neurons.

A Schematic illustration of the strategy to knock down Gper1 in the post-synaptic neurons of S1HL-SDH projections in a Cre-dependent manner (Up) and the diagram showing the timeline of virus injection, CCI surgery and behavioral tests (Down).

B-D Behavioral tests of basic nociception and 14 days after CCI surgery in Von Frey tests **(B)**, Brush tests **(C)** and Heat tests **(D)** in mice of both genders (n = 6 mice for each group).

E Immunochemical detection of the localization of virus expression (Green). Scale bars: 100 μm.

F Quantitative PCR analysis of *Gper1* mRNA in SDH (n = 3 mice for each group).

Data information: in **(B, C)**, $^{**}P < 0.01$; $^{***}P < 0.001$; $^{****}P < 0.0001$ (two-way ANOVA with Turkey's multiple comparisons test). In **(D)**, $^{*}P < 0.05$; $^{**}P < 0.01$; $^{****}P < 0.0001$ (one-way ANOVA with Turkey's multiple comparisons test). In **(F)**, $^{*}P < 0.05$ (one-way ANOVA with Turkey's multiple comparisons test). All data are presented as mean ± SEM.

Supplemental Figures and Legends

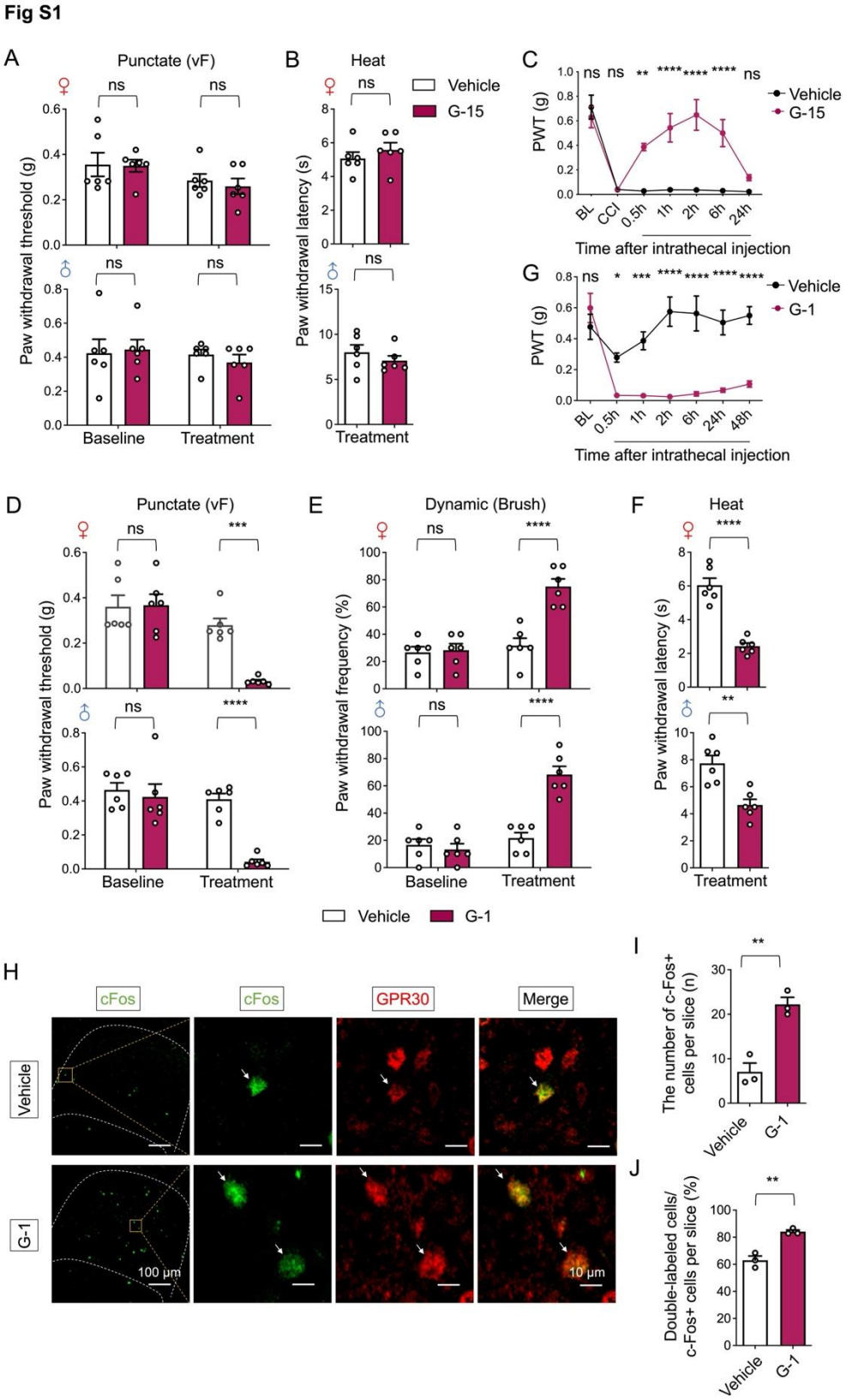

Figure S1 - Spinal inhibition of GPR30 did not change the basic nociception while spinal

activation of GPR30 mimicked neuropathic pain symptoms in naïve mice

A, B Behavioral tests of nociception before and after intrathecal injection of G-15 or vehicle in Von Frey tests **(A)** and Heat tests **(B)** in naive mice of both genders (n = 6 mice for each group).

C Time course of Von Frey tests after intrathecal injection of G-15 or vehicle in CCI mice (n = 6 mice for each group).

D-F Behavioral tests of nociception before and after intrathecal injection of G-1 or vehicle in Von Frey tests **(D)**, Brush tests **(E)** and Heat tests **(F)** in naive mice of both genders (n = 6 mice for each group).

G Time course of Von Frey tests after intrathecal injection of G-1 or vehicle in naive mice (n = 6 mice for each group).

H Immunochemical detection of c-Fos (Green) and GPR30 (Red). Scale bars: 100 μm. Boxed area of images is enlarged on the right. Scale bars: 10 μm. White arrows indicate double-positive cells.

I Total number of c-Fos positive neurons in the SDH per section (n = 3 mice for each group).

J Percentage of c-Fos positive neurons expressing GPR30 (n = 3 mice for each group).

Data information: in **(A)**, ns = not significant (two-way ANOVA with Turkey's multiple comparisons test). In **(B)**, ns = not significant (Unpaired Student's t-test). In **(C)**, $^{**}P < 0.01$; $^{****}P < 0.0001$; ns = not significant (two-way ANOVA with Turkey's multiple comparisons test). In **(D, E)**, $^{***}P < 0.001$; $^{****}P < 0.0001$; ns = not significant. (two-way ANOVA with Turkey's multiple comparisons test). In **(F)**, $^{**}P < 0.01$; $^{****}P < 0.0001$ (Unpaired Student's t-test). In **(G)**, $^{*}P < 0.05$; $^{***}P < 0.001$; $^{****}P < 0.0001$; ns = not significant (two-way

ANOVA with Turkey's multiple comparisons test). In **(I, J)**, $^{**}P < 0.01$ (Unpaired Student's t-test).All data are presented as mean ± SEM.

Fig S2

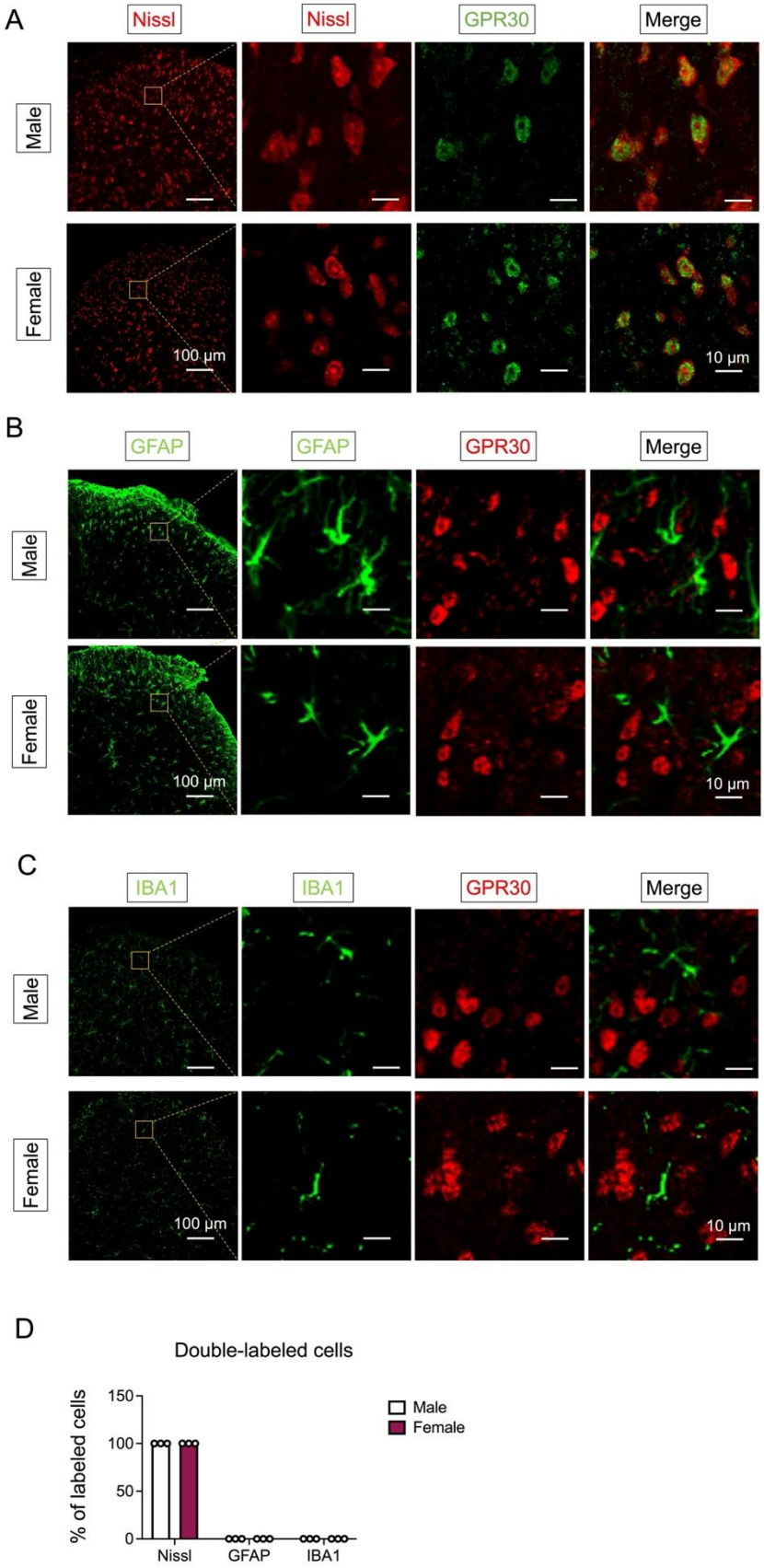
A
Nissl
Nissl
GPR30
Merge
Male
Female
100 µm
10 µm
B
GFAP
GFAP
GPR30
Merge
Male
Female
100 µm
10 µm
C
IBA1
IBA1
GPR30
Merge
Male
Female
100 µm
10 µm
D
Double-labeled cells
% of labeled cells
150
100
50
0
Nissl
GFAP
IBA1
Male
Female

952

Figure S2 - GPR30 was mainly expressed in the spinal neurons.

A Double-staining of GPR30 (Green) with Nissl (Red) in male (up) and female mice (down). Scale bars: 100 μm. Boxed area of images is enlarged on the right. Scale bars: 10 μm.

B Double-staining of GPR30 (Red) with GFAP (Green) in male (up) and female mice (down). Scale bars: 100 μm. Boxed area of images is enlarged on the right. Scale bars 10 μm.

C Double-staining of GPR30 (Red) with IBA1 (Green) in male (up) and female mice (down). Scale bars: 100 μm. Boxed area of images is enlarged on the right. Scale bars: 10 μm.

D Percentage of GPR30 expressed in neurons, astrocytes and microglia in both genders of mice (n = 3 mice for each group).

Data information: in **(D)**, data are presented as mean ± SEM.

Fig S3

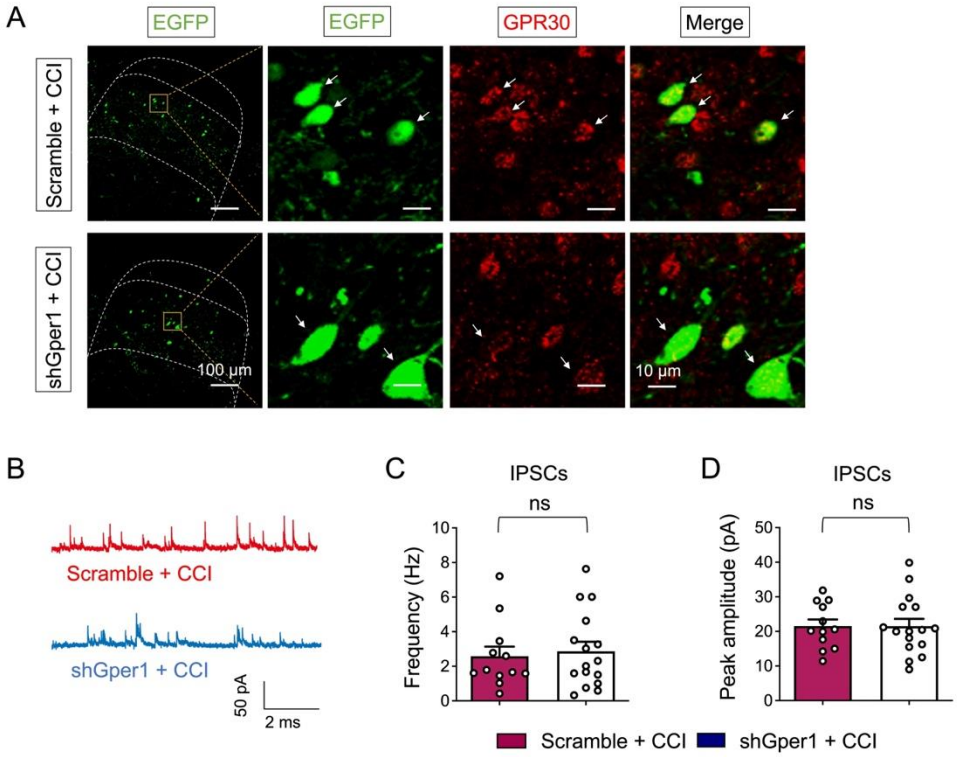

Figure S3 - Knockdown of GPR30 in spinal CCK$^+$ neurons did not change the sIPSC in CCI mice.

A Immunohistochemical detection of GPR30 (Red) and shRNA (Green) in mice with virus injection. Note that the intensity of GPR30 fluorescence is less in shGper1-EGFP$^+$ cells than that in scramble-EGFP$^+$ cells. Scale bars: 100 μm. Boxed area of image is enlarged on the right. Scale bars: 10 μm.

B Representative spontaneous IPSCs in CCK-EGFP neurons.

C The frequency of spontaneous IPSCs (n = 12-16 cells from 5 mice).

D The peak amplitude spontaneous IPSCs (n = 12-16 cells from 5 mice).

Data information: in **(C, D)**, ns = not significant (Unpaired Student's t-test). All data are presented as mean ± SEM.

Fig S4

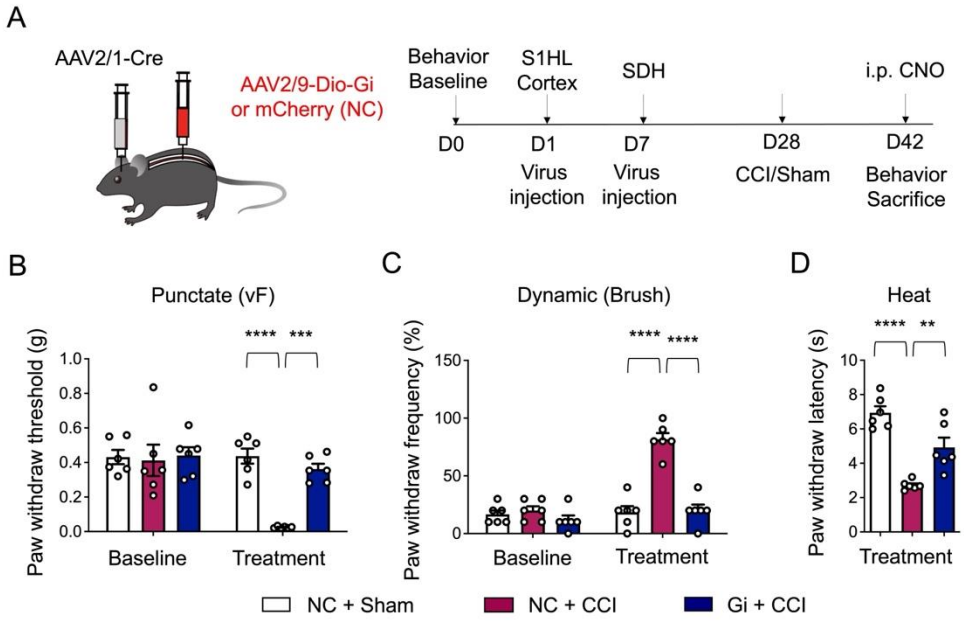

Figure S4 - CCI-induced neuropathic pain was relieved by chemogenetic inhibition of S1-SDH post-synaptic neurons.

A Schematic illustration of the strategy for identifying the post-synaptic neurons of S1HL-SDH projections in SDH (Left) and diagram showing the timeline of AAV2/1 injection in the S1HL cortex, AAV2/9 injection in the spinal dorsal horn, CCI surgery and behavioral tests (Right).

B-D Behavioral tests of basic nociception, 14 days after CCI surgery along with intraperitoneal injection of CNO in Von Frey tests **(B)**, Brush tests **(C)** and Heat tests **(D)** in mice (n = 6 mice per group).

Data information: In **(B, C)**, ***$P < 0.001$; ****$P < 0.0001$. (two-way ANOVA with Turkey's multiple comparisons test). In **(D)**, **$P < 0.01$; ****$P < 0.0001$ (one-way ANOVA with Turkey's multiple comparisons test). All data are presented as mean ± SEM